Comparison of human versus mouse CYP1A1 and CYP1A2 TCDD-induced enzyme activities in liver

For BaP hydroxylase and EROD as two activities associated predominantly with CYP1A1, the correlations between enzyme activities (Fig. 3A) and mRNA levels (Fig. 1A) are extremely variable for BaP hydroxylase but quite consistent for EROD activity. Thus, B6 mice exhibit one-half as much TCDD-induced BaP hydroxylase activity (per unit of mCYP1A1 mRNA) as *uPA/SCID* mice (Table 2). The B6 mouse shows ~170 times more induced BaP hydroxylase activity (per unit of mCYP1A1 mRNA), compared with the *hCYP1A1_1A2_Cyp1a1/1a2(−/−)* mouse's induced BaP hydroxylase activity (per unit of hCYP1A1 mRNA). Chimeric mice exhibit ~6.2-fold more induced BaP hydroxylase activity (per unit of hCYP1A1 mRNA) than *hCYP1A1_1A2_Cyp1a1/1a2(−/−)* mice (Table 2). The *uPA/SCID* mouse shows ~42 times more induced BaP hydroxylase activity (per unit of mCYP1A1 mRNA), compared with the chimeric mouse's induced BaP hydroxylase activity (per unit of hCYP1A1 mRNA).

In contrast, B6 mice display about the same amount of TCDD-induced EROD activity (per unit of mCYP1A1 mRNA) as *uPA/SCID* mice (Table 2). The B6 mouse shows ~54 times more induced EROD activity (per unit of mCYP1A1 mRNA), compared with the *hCYP1A1_1A2_Cyp1a1/1a2(−/−)* mouse's induced EROD activity (per unit of hCYP1A1 mRNA). Chimeric mice exhibit ~1.7 times more induced EROD activity (per unit of hCYP1A1 mRNA) than *hCYP1A1_1A2_Cyp1a1/1a2(−/−)* mice (Table 2). The *uPA/SCID* mouse shows ~39 times more induced EROD activity (per unit of mCYP1A1 mRNA), compared with the chimeric mouse's induced EROD activity (per unit of hCYP1A1 mRNA).

Why does the humanized *hCYP1A1_1A2_Cyp1a1/1a2(−/−)* mouse carry so little enzyme activity toward BaP, compared with the chimeric mouse? This difference can be explained from the human hepatocyte-replacement rate (73%–83%) in chimeric mice. The liver of chimeric mice carries 73%–83% human hepatocytes, which exhibit extremely low BaP hydroxylase activity.

For acetanilide 4-hydroxylase and MROD as two activities associated predominantly with CYP1A2, the correlations between enzyme activities (Fig. 3B) and mRNA levels (Fig. 1B) are very much consistent with one another. B6 mice show virtually the same amount of TCDD-induced acetanilide 4-hydroxylase activity (per unit of mCYP1A2 mRNA) as *uPA/SCID* mice (Table 2). The B6 mouse shows about the same amount of induced acetanilide 4-hydroxylase activity (per unit of mCYP1A2 mRNA), compared with the *hCYP1A1_1A2_Cyp1a1/1a2(−/−)* mouse's induced acetanilide 4-hydroxylase activity (per unit of hCYP1A2 mRNA). Chimeric mice exhibit twice as much induced acetanilide 4-hydroxylase activity (per unit of hCYP1A2 mRNA) than *hCYP1A1_1A2_Cyp1a1/1a2(−/−)* mice (Table 2). The chimeric mouse shows ~2.3-fold more induced acetanilide 4-hydroxylase activity (per unit of mCYP1A2 mRNA), compared with the *uPA/SCID* mouse's induced acetanilide 4-hydroxylase activity (per unit of hCYP1A2 mRNA).

B6 mice exhibit one-half as much TCDD-induced MROD activity (per unit of mCYP1A2 mRNA) as *uPA/SCID* mice (Table 2). The *hCYP1A1_1A2_Cyp1a1/1a2(−/−)* mouse shows ~2-fold more induced MROD activity (per unit of mCYP1A2 mRNA), compared with the B6 mouse's induced MROD activity (per unit of hCYP1A2 mRNA). The *hCYP1A1_1A2_Cyp1a1/1a2(−/−)* mice exhibit ~2.4 times more in-

Table 2
Ratios of mouse liver TCDD-induced enzymic activities per unit of mRNA*.

	mCYP1A1		hCYP1A1	
B6 mouse	7600 ± 2700	h1A1_1A2	44 ± 13	BaP hydroxylase
uPA/SCID	11,400 ± 3000	Chimera	270 ± 62	
B6 mouse	230 ± 64	h1A1_1A2	4.3 ± 1.3	EROD activity
uPA/SCID	290 ± 95	Chimera	7.4 ± 3.1	

	mCYP1A2		hCYP1A2	
B6 mouse	490 ± 84	h1A1_1A2	600 ± 220	Acetanilide
uPA/SCID	510 ± 200	Chimera	1200 ± 390	4-hydroxylase
B6 mouse	5.4 ± 1.0	h1A1_1A2	14 ± 5.5	MROD activity
uPA/SCID	13 ± 5.2	Chimera	5.6 ± 0.3	

* For BaP hydroxylase, these ratios represent FU/min/mg protein divided by mRNA × 10^9 per μg total RNA. For the other three enzyme activities, these ratios represent pmol/min/mg protein divided by mRNA × 10^9 per μg total RNA. Values are expressed as means ± S.E.

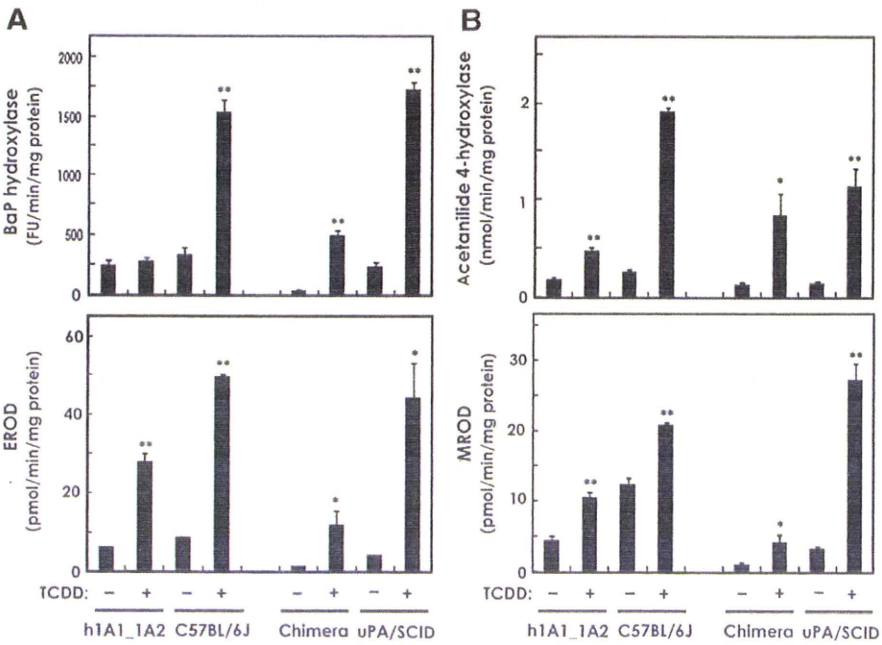

Fig. 3. (A) BaP hydroxylase and EROD activity (both representing largely CYP1A1), and (B) acetanilide 4-hydroxylase and MROD activity (both representing largely CYP1A2) in liver microsomes from the same mouse lines as in Fig. 1. FU, fluorescent units. *$P < 0.05$ and **$P < 0.01$, when comparing TCDD-pretreated with no pretreatment.

duced MROD activity (per unit of hCYP1A2 mRNA) than chimeric mice (Table 2). The *uPA/SCID* mouse shows twice as much induced MROD activity (per unit of mCYP1A2 mRNA), compared with the chimeric mouse's induced MROD activity (per unit of hCYP1A2 mRNA). Expression of CYP1A2 catalytic activity, relative to CYP1A2 mRNA levels, in the humanized *hCYP1A1_1A2_Cyp1a1/1a2(−/−)* and chimeric mouse lines is therefore very robust and within 2-fold similar to that expressed in mouse liver.

Comparison of human versus mouse CYP1A1 and CYP1A2 mRNA levels in hepatoma-derived cell culture lines

Animal rights' activists have urged scientists to study physiological functions in cell cultures rather than using live laboratory animals. Many studies have shown, however, that parameters found in cell culture do not accurately reflect what happens in the intact animal.

How does the expression of the *CYP1A1* and *CYP1A2* genes in intact liver compare with that in hepatoma-derived established cell lines? In HepG2 cells (Fig. 4A), human basal CYP1A1 mRNA was negligible, whereas human TCDD-induced CYP1A1 mRNA gave $\sim 5.4 \times 10^9$ copy numbers (per μg total RNA). In Hepa-1c1c7 cells (Fig. 4A), mouse basal versus TCDD-induced CYP1A1 mRNA showed $\sim 0.35 \times 10^8$ and $\sim 1.9 \times 10^8$ copy numbers, respectively. Mouse CYP1A1 mRNA was not detected in HepG2, and human CYP1A1 mRNA was not detected in Hepa-1c1c7 cells.

In HepG2 cells (Fig. 4B), human basal versus TCDD-induced CYP1A2 mRNA gave $\sim 0.27 \times 10^6$ and $\sim 4.8 \times 10^6$ copy numbers, respectively. In Hepa-1c1c7 cells (Fig. 4B), mouse basal versus TCDD-induced CYP1A2 mRNA showed $\sim 0.14 \times 10^6$ and $\sim 1.2 \times 10^6$ copies, respectively. Mouse CYP1A2 mRNA was not detected in HepG2, and human CYP1A2 mRNA was not detected in Hepa-1c1c7 cells.

Thus, in livers of the *hCYP1A1_1A2_Cyp1a1/1a2(−/−)* and chimeric mice, the copy number of human induced CYP1A1 mRNA is 7.5 and 2.6 times, respectively, greater than that of human induced CYP1A2 mRNA. On the other hand, in the HepG2 liver-derived established cell line, the copy number of human induced CYP1A1 mRNA is more than 1100 times greater than that of human induced CYP1A2 mRNA. In livers of the B6 and *uPA/SCID* mice, the copy number of mouse induced CYP1A2 mRNA is 40-fold and 20-fold, respectively, greater than that of mouse induced CYP1A1 mRNA; in contrast, in the Hepa-1c1c7 established cell line, the copy number of mouse induced CYP1A1 mRNA is almost 1600-fold greater than that of mouse maximally-inducible CYP1A2 mRNA. This decline in *CYP1A2* gene expression seen in established cell lines reflects the well-known fact that numerous "housekeeping" genes such as *CYP1A2* are extinguished, or are greatly decreased in expression—in tumor cells as well as "established", or transformed, cell lines in culture (Owens et al., 1975; Nebert, 2006). However, such suppression often does not occur for the *CYP1A1* gene in differentiated tumors, including the HepG2 and Hepa-1c1c7 hepatoma-derived cell lines (Owens et al., 1975; Nebert, 2006).

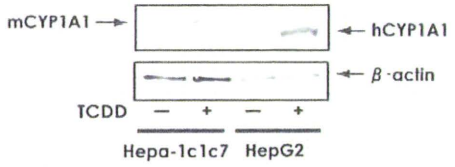

Fig. 5. Western immunoblot analysis of mouse versus human hepatic CYP1A1 and CYP1A2 proteins in the same cell culture lines as in Fig. 4. Everything is the same as that described for the Western blot in Fig. 2. The amount of cell culture protein (10 μg) loaded per lane was constant for all lanes.

Comparison of human versus mouse CYP1A1 and CYP1A2 protein levels in hepatoma-derived cell culture lines

We carried out Western immunoblots of Hepa-1c1c7 and HepG2 cells, control versus TCDD-pretreated (Fig. 5). The human CYP1A1 protein appears to migrate more rapidly than the mouse CYP1A1 protein. We believe the level of CYP1A2 protein was so low that it was not detected in either established hepatoma cell line.

Comparison of human versus mouse CYP1A1 and CYP1A2 TCDD-induced enzyme activities in hepatoma-derived cell culture lines

Different from what was found in mouse liver, the correlations between enzyme activities (Fig. 6A) and mRNA levels (Fig. 4A) are extremely variable for EROD activity but more consistent for BaP

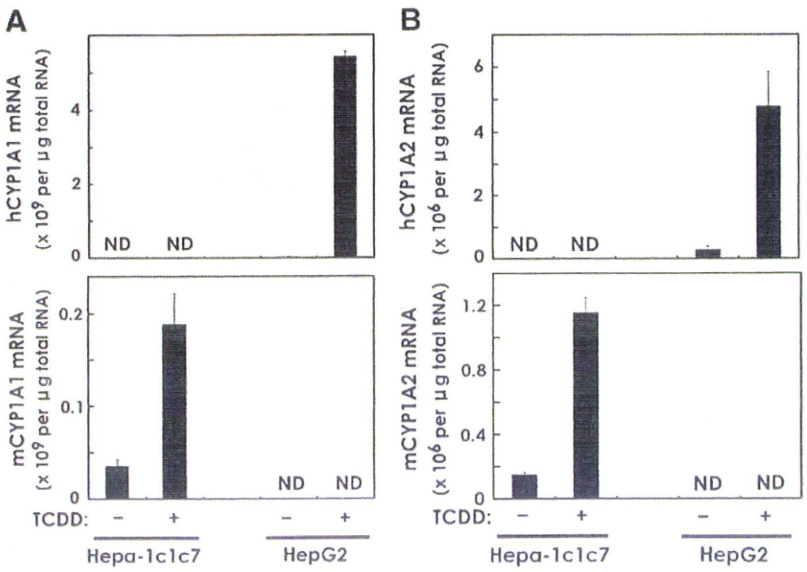

Fig. 4. Human (*upper panels*) versus mouse (*lower panels*) CYP1A1 (A) and CYP1A2 (B) mRNA copy numbers in mouse Hepa-1c1c7 cells and human HepG2 cells—with, versus without, TCDD exposure (10 nM for 24 h) in culture. Abbreviations are the same as those in Fig. 1.

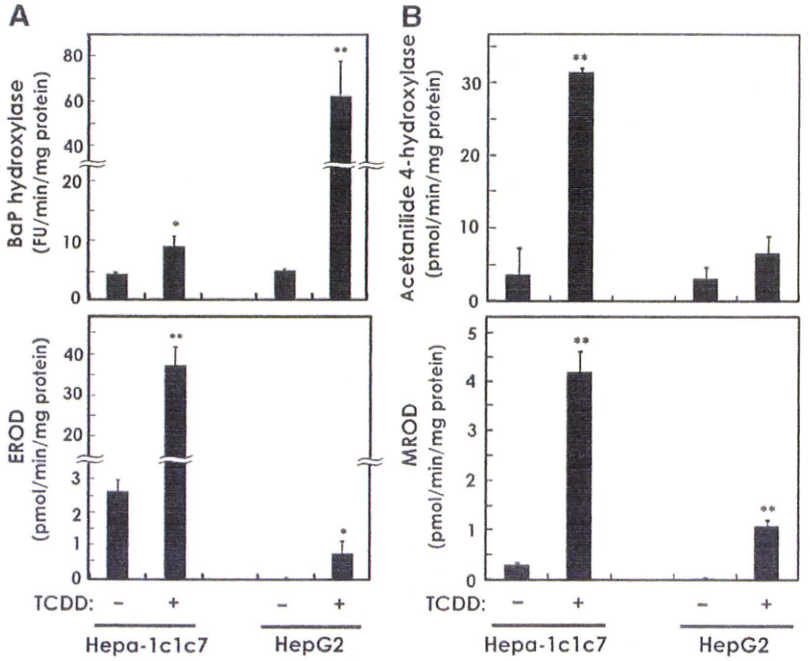

Fig. 6. (A) BaP hydroxylase and EROD activity (both representing largely CYP1A1), and (B) acetanilide 4-hydroxylase and MROD activity (both representing largely CYP1A2) in the same cell culture lines as in Fig. 4. $^{*}P<0.05$ and $^{**}P<0.01$, when comparing TCDD-pretreated with no pretreatment.

hydroxylase activity. Hepa-1c1c7 cells show ~4.8 times more TCDD-induced BaP hydroxylase activity (per unit of mCYP1A1 mRNA) than HepG2 cells exhibit for induced BaP hydroxylase activity (per unit of hCYP1A1 mRNA) (Table 3). Hepa-1c1c7 cells show ~1500 times more TCDD-induced EROD activity (per unit of mCYP1A1 mRNA) than HepG2 cells exhibit for induced EROD activity (per unit of hCYP1A1 mRNA). For whatever reason, HepG2 cells do not display very high induced BaP hydroxylase activity, and their induced EROD activity is extremely low.

For acetanilide 4-hydroxylase and MROD as two activities associated predominantly with CYP1A2, the correlations between enzyme activities (Fig. 6B) and mRNA levels (Fig. 6B) are better than those with CYP1A1. Hepa-1c1c7 cells show ~16-fold more TCDD-induced acetanilide 4-hydroxylase activity (per unit of mCYP1A2 mRNA) than HepG2 cells exhibit for induced acetanilide 4-hydroxylase activity (per unit of hCYP1A2 mRNA) (Table 3). Hepa-1c1c7 cells show ~15-fold more TCDD-induced MROD activity (per unit of mCYP1A2 mRNA) than HepG2 cells exhibit for induced MROD activity (per unit of hCYP1A2 mRNA). Therefore, HepG2 cells do not express either CYP1A1 or CYP1A2 activities nearly as robustly as do Hepa-1c1c7 cells.

Table 3
Ratios of hepatoma-derived cell line TCDD-induced enzymic activities per unit of mRNA*.

	mCYP1A1		hCYP1A1	
Hepa-1c1c7	55 ± 21	HepG2	11 ± 2.5	BaP hydroxylase
Hepa-1c1c7	210 ± 48	HepG2	0.14 ± 0.06	EROD activity
	mCYP1A2		**hCYP1A2**	
Hepa-1c1c7	27,000 ± 2400	HepG2	1800 ± 930	Acetanilide 4-hydroxylase
Hepa-1c1c7	3700 ± 480	HepG2	250 ± 85	MROD activity

* For BaP hydroxylase, these ratios represent FU/min/mg protein divided by mRNA × 10^9 per μg total RNA. For the other three enzyme activities, these ratios represent pmol/min/mg protein divided by mRNA × 10^9 per μg total RNA. Values are expressed as means ± S.E.

Conclusions

In this study we have measured the amount of variability between human and mouse CYP1A mRNA and protein levels and corresponding enzyme activities in the humanized *hCYP1A1_1A2_Cyp1a1/1a2(−/−)* and chimeric *uPA/SCID* lines, by comparing these parameters with those seen in wild-type mice from which these two lines were derived. We have also compared these mRNA and protein levels and corresponding enzyme activities in mouse hepatoma-derived Hepa-1c1c7 and human hepatoblastoma-derived HepG2 established cell culture lines. Clearly, the CYP1A1/CYP1A2 activity ratios in these hepatoma-derived established cell lines are not accurate indicators of those in liver from the intact mouse. Undoubtedly, this discrepancy is primarily caused by the dramatically lowered CYP1A2 mRNA levels—presumably due to "extinction" of the normal expression of the *CYP1A2* gene in these hepatoma-derived established cell lines. Not only very low CYP1A2 enzyme activity per unit of mRNA was seen in both Hepa-1c1c7 and HepG2 cells, but also low CYP1A1 enzyme activity per unit of hCYP1A1 mRNA was found in HepG2 cells.

Comparing liver of the two humanized mouse lines with liver of mice from which these two humanized lines were derived was most disturbing when one examined CYP1A1-specific (BaP and ethoxyresorufin) and CYP1A2-specific (acetanilide and methoxyresorufin) substrates metabolized—per unit of mCYP1A1, hCYP1A1, mCYP1A2 or hCYP1A2 mRNA. The hCYP1A1 in mouse liver was between 38 and more than 170 times less efficient than mCYP1A1 in the hydroxylation of BaP and about 54-fold less efficient in EROD activity. In contrast, hCYP1A2 in mouse liver appeared to function nearly equivalent to mCYP1A2 in wild-type mouse liver.

The levels of human CYP1A1 and CYP1A2 mRNA in both humanized mouse lines appear to be quite compatible with what might be expected among individual persons in any human population. It is very clear, however, that substrate specificity varies widely, independent of human versus mouse CYP1A1/1A2 mRNA or protein concentrations. Nevertheless, keeping this caveats in mind, both of these lines should still be useful for studies in human risk assessment, toxicology, pharmacology, and other medical subspecialties.

Note added in proof

A recent study (Wilson et al., 2008) is directly relevant to the problems addressed in our present manuscript. This study involves Tc1 hepatocytes, derived from an aneuploid mouse strain carrying human chromosome (Chr) 21 in addition to the entire mouse genome. The authors compared the regulation of human genes in Tc1 cells to that of the mouse orthologous genes in these same cells, using mouse wild-type versus human wild-type cells as controls. Regulation in the nuclei of Tc1 cells was compared at three levels: binding of transcription factors to DNA, modification of histones, and gene expression. The binding patterns of HNF1α, HNF4α and HNF6 on human Chr 21 in Tc1 cells matched closely those seen in human wild-type cells, rather than those seen in mouse wild-type cells. Similarly, histone modifications–as well as gene expression (the amount of mRNA transcribed)–showed human-specific, instead of mouse-specific, patterns on human Chr 21 in Tc1 cells. The authors concluded that it is the regulatory DNA sequence, rather than any other species-specific factor, which is the single most important determinant of gene expression (Wilson et al., 2008).

Acknowledgments

We thank our colleagues for many fruitful discussions and careful readings of this manuscript. Supported, in part, by the Ministry of Education, Science, Sports & Culture, Japan (Grant-in-Aid for Scientific Research on Priority Areas, 18077005 to S.U. and M.M.), and Nihon University Joint Research Grant for 2007 (S.U.), and NIH Grants R01 ES014403 (D.W.N.) and P30 ES06096 (D.W.N.).

References

Aoyama, T., Gonzalez, F.J., Gelboin, H.V., 1989. Human cDNA-expressed cytochrome P450 1A2: mutagen activation and substrate specificity. Mol. Carcinog. 2, 192–198.
Bedell, M.A., Jenkins, N.A., Copeland, N.G., 1996. Good genes in bad neighbourhoods. Nat. Genet. 12, 229–232.
Bennett, L.M., McAllister, K.A., Blackshear, P.E., Malphurs, J., Goulding, G., Collins, N.K., Ward, T., Bunch, D.O., Eddy, E.M., Davis, B.J., Wiseman, R.W., 2000. *Brca2*-null embryonic survival is prolonged on the BALB/c genetic background. Mol. Carcinog. 28, 174–183.
Bernhard, H.P., Darlington, G.J., Ruddle, F.H., 1973. Expression of liver phenotypes in cultured mouse hepatoma cells: synthesis and secretion of serum albumin. Dev. Biol. 35, 83–96.
Berthou, F., Guillois, B., Riche, C., Dreano, Y., Jacqz-Aigrain, E., Beaune, P.H., 1992. Interspecies variations in caffeine metabolism related to cytochrome P450 1A enzymes. Xenobiotica 22, 671–680.
Bonyadi, M., Rusholme, S.A., Cousins, F.M., Su, H.C., Biron, C.A., Farrall, M., Akhurst, R.J., 1997. Mapping of a major genetic modifier of embryonic lethality in *Tgfb1*(−/−) knockout mice. Nat. Genet. 15, 207–211.
Burke, M.D., Mayer, R.T., Kouri, R.E., 1977. 3-Methylcholanthrene-induced monooxygenase (O-deethylation) activity of human lymphocytes. Cancer Res. 37, 460–463.
Cheung, C., Ma, X., Krausz, K.W., Kimura, S., Feigenbaum, L., Dalton, T.P., Nebert, D.W., Idle, J.R., Gonzalez, F.J., 2005. Differential metabolism of 2-amino-1-methyl-6-phenylimidazo[4,5-*b*]pyridine (PhIP) in mice humanized for CYP1A1 and CYP1A2. Chem. Res. Toxicol. 18, 1471–1478.
Cranston, A., Fishel, R., 1999. Female embryonic lethality in *Msh2–Trp53* nullizygous mice is strain-dependent. Mamm. Genome 10, 1020–1022.
Dalton, T.P., Dieter, M.Z., Matlib, R.S., Childs, N.L., Shertzer, H.G., Genter, M.B., Nebert, D.W., 2000. Targeted knockout of *Cyp1a1* gene does not alter hepatic constitutive expression of other genes in the mouse [*Ah*] battery. Biochem. Biophys. Res. Commun. 267, 184–189.
Dearfield, K.L., Jacobson-Kram, D., Brown, N.A., Williams, J.R., 1983. Evaluation of a human hepatoma cell line as a target cell in genetic toxicology. Mutat. Res. 108, 437–449.
Derkenne, S., Curran, C.P., Shertzer, H.G., Dalton, T.P., Dragin, N., Nebert, D.W., 2005. Theophylline pharmacokinetics: comparison of *Cyp1a1*(−/−) and *Cyp1a2*(−/−) knockout mice, humanized *hCYP1A1_1A2* knock-in mice lacking either the mouse *Cyp1a1* or *Cyp1a2* gene, and *Cyp1*(+/+) wild-type mice. Pharmacogenet. Genomics 15, 503–511.
Dragin, N., Uno, S., Wang, B., Dalton, T.P., Nebert, D.W., 2007. Generation of 'humanized' *hCYP1A1_1A2_Cyp1a1/1a2*(−/−) mouse line. Biochem. Biophys. Res. Commun. 359, 635–642.
Eaton, D.L., Gallagher, E.P., Bammler, T.K., Kunze, K.L., 1995. Role of cytochrome P450 1A2 in chemical carcinogenesis: implications for human variability in expression and enzyme activity. Pharmacogenetics 5, 259–274.
Giannini, C., Morosan, S., Tralhao, J.G., Guidotti, J.E., Battaglia, S., Mollier, K., Hannoun, L., Kremsdorf, D., Gilgenkrantz, H., Charneau, P., 2003. A highly efficient, stable, and rapid approach for ex vivo human liver gene therapy via a FLAP lentiviral vector. Hepatology 38, 114–122.
Hamm, J.T., Ross, D.G., Richardson, V.M., Diliberto, J.J., Birnbaum, L.S., 1998. Methoxyresorufin: an inappropriate substrate for CYP1A2 in the mouse. Biochem. Pharmacol. 56, 1657–1660.
Inaba, Y., Yamamoto, K., Yoshimoto, N., Matsunawa, M., Uno, S., Yamada, S., Makishima, M., 2007. Vitamin D3 derivatives with adamantane or lactone ring side chains are cell type-selective vitamin D receptor modulators. Mol. Pharmacol. 71, 1298–1311.
Jiang, Z., Dalton, T.P., Jin, L., Wang, B., Tsuneoka, Y., Shertzer, H.G., Deka, R., Nebert, D.W., 2005. Toward the evaluation of function in genetic variability: characterizing human SNP frequencies and establishing BAC-transgenic mice carrying the human *CYP1A1_CYP1A2* locus. Hum. Mutat. 25, 196–206.
Katoh, M., Tateno, C., Yoshizato, K., Yokoi, T., 2008. Chimeric mice with humanized liver. Toxicology 246, 9–17.
Lindberg, R.L., Negishi, M., 1989. Alteration of mouse cytochrome P450coh substrate specificity by mutation of a single amino-acid residue. Nature 339, 632–634.
Milot, E., Fraser, P., Grosveld, F., 1996. Position effects and genetic disease. Trends Genet. 12, 123–126.
Muller, K., Heller, H., Doerfler, W., 2001. Foreign DNA integration. Genome-wide perturbations of methylation and transcription in the recipient genomes. J. Biol. Chem. 276, 14271–14278.
Nebert, D.W., 1989. The *Ah* locus: genetic differences in toxicity, cancer, mutation, and birth defects. Crit. Rev. Toxicol. 20, 153–174.
Nebert, D.W., 2006. Comparison of gene expression in cell culture to that in the intact animal: relevance to drugs and environmental toxicants. Am. J. Physiol., Cell Physiol. 290, C37–C41.
Nebert, D.W., Dalton, T.P., 2006. The role of cytochrome P450 enzymes in endogenous signalling pathways and environmental carcinogenesis. Nat. Rev., Cancer 6, 947–960.
Nebert, D.W., Gelboin, H.V., 1968. Substrate-inducible microsomal aryl hydroxylase in mammalian cell culture. I. Assay and properties of induced enzyme. J. Biol. Chem. 243, 6242–6249.
Nebert, D.W., Dalton, T.P., Okey, A.B., Gonzalez, F.J., 2004. Role of aryl hydrocarbon receptor-mediated induction of the CYP1 enzymes in environmental toxicity and cancer. J. Biol. Chem. 279, 23847–23850.
Nelson, D.R., Koymans, L., Kamataki, T., Stegeman, J.J., Feyereisen, R., Waxman, D.J., Waterman, M.R., Gotoh, O., Coon, M.J., Estabrook, R.W., Gunsalus, I.C., Nebert, D.W., 1996. P450 superfamily: update on new sequences, gene mapping, accession numbers and nomenclature. Pharmacogenetics 6, 1–42.
Nelson, D.R., Zeldin, D.C., Hoffman, S.M., Maltais, L.J., Wain, H.M., Nebert, D.W., 2004. Comparison of cytochrome P450 (*CYP*) genes from the mouse and human genomes, including nomenclature recommendations for genes, pseudogenes, and alternative-splice variants. Pharmacogenetics 14, 1–18.
Nichols, R.C., Cooper, S., Trask, H.W., Gorman, N., Dalton, T.P., Nebert, D.W., Sinclair, J.F., Sinclair, P.R., 2003. Uroporphyrin accumulation in hepatoma cells expressing human or mouse CYP1A2: relation to the role of CYP1A2 in human porphyria cutanea tarda. Biochem. Pharmacol. 65, 545–550.
Olson, E.N., Arnold, H.H., Rigby, P.W., Wold, B.J., 1996. Know your neighbors: three phenotypes in null mutants of the myogenic bHLH gene *Mrf4*. Cell 85, 1–4.
Owens, I.S., Niwa, A., Nebert, D.W., 1975. In: Gerschenson, L.E., Thompson, E.B. (Eds.), Expression of Aryl Hydrocarbon Hydroxylase Induction in Liver- and Hepatoma-Derived Cell Cultures. Academic Press, New York, NY, pp. 378–401.
Shertzer, H.G., Nebert, D.W., Senft, A.P., Dingledein, M., Genter, M.B., Dalton, T.P., 2001. Spectrophotometric assay for acetanilide 4-hydroxylase, an estimate of CYP1A2 enzyme activity. Toxicol. Meth. 11, 81–88.
Shi, Z., Chen, Y., Dong, H., Amos-Kroohs, R.M., Nebert, D.W., 2008. Generation of 'humanized' *hCYP1A1_1A2_Cyp1a1/1a2*(−/−)*_Ahr*^{d} mouse line harboring the poor-affinity aryl hydrocarbon receptor. Biochem. Biophys. Res. Commun. 376, 775–780.
Tateno, C., Yoshizane, Y., Saito, N., Kataoka, M., Utoh, R., Yamasaki, C., Tachibana, A., Soeno, Y., Asahina, K., Hino, H., Asahara, T., Yokoi, T., Furukawa, T., Yoshizato, K., 2004. Near completely humanized liver in mice shows human-type metabolic responses to drugs. Am. J. Pathol. 165, 901–912.
Tavangar, K., Hoffman, A.R., Kraemer, F.B., 1990. A micromethod for the isolation of total RNA from adipose tissue. Anal. Biochem. 186, 60–63.
Turesky, R.J., 2005. Interspecies metabolism of heterocyclic aromatic amines and the uncertainties in extrapolation of animal toxicity data for human risk assessment. Mol. Nutr. Food Res. 49, 101–117.
Uno, S., Dalton, T.P., Dragin, N., Curran, C.P., Derkenne, S., Miller, M.L., Shertzer, H.G., Gonzalez, F.J., Nebert, D.W., 2006. Oral benzo[*a*]pyrene in *Cyp1* knockout mouse lines: CYP1A1 important in detoxication, CYP1B1 metabolism required for immune damage independent of total-body burden and clearance rate. Mol. Pharmacol. 69, 1103–1114.
Uno, S., Dragin, N., Miller, M.L., Dalton, T.P., Gonzalez, F.J., Nebert, D.W., 2008. Basal and inducible CYP1 mRNA quantitation and protein localization throughout the mouse gastrointestinal tract. Free Radic. Biol. Med. 44, 570–583.
Wilson, M.D., Barbosa-Morais, N.L., Schmidt, D., Conboy, C.M., Vanes, L., Tybulewicz, V.L., Fisher, E.M., Tavaré, S., Odom, D.T., 2008. Species-specific transcription in mice carrying human chromosome 21. Science 322, 434–438.
Winer, J., Jung, C.K., Shackel, I., Williams, P.M., 1999. Development and validation of real-time quantitative reverse transcriptase-polymerase chain reaction for monitoring gene expression in cardiac myocytes in vitro. Anal. Biochem. 270, 41–49.

Inhibition of Transforming Growth Factor β Signaling by Halofuginone as a Modality for Pancreas Fibrosis Prevention

Orit Zion, MSc, Olga Genin, MSc,* Norifumi Kawada, MD,† Katsutoshi Yoshizato, MD,‡ Suzy Roffe, MsC,§ Arnon Nagler, MD,|| Juan L. Iovanna, MD, PhD,¶ Orna Halevy, PhD,§ and Mark Pines, PhD**

Objectives: Chronic pancreatitis is characterized by inflammation and fibrosis. We evaluated the efficacy of halofuginone, an inhibitor of collagen synthesis and myofibroblast activation, in preventing cerulein-induced pancreas fibrosis.

Methods: Collagen synthesis was evaluated by in situ hybridization and staining. Levels of prolyl 4-hydroxylase β (P4Hβ), cytoglobin/stellate cell activation–associated protein (Cygb/STAP), transgelin, tissue inhibitors of metalloproteinases, serum response factor, transforming growth factor β (TGFβ), Smad3, and pancreatitis-associated protein 1 (PAP-1) were determined by immunohistochemistry. Metalloproteinase activity was evaluated by zymography.

Results: Halofuginone prevented cerulein-dependent increase in collagen synthesis, collagen cross-linking enzyme P4Hβ, Cygb/STAP, and tissue inhibitors of metalloproteinase 2. Halofuginone did not affect TGFβ levels in cerulein-treated mice but inhibited serum response factor synthesis and Smad3 phosphorylation. In culture, halofuginone inhibited pancreatic stellate cell (PSC) proliferation and TGFβ-dependent increase in Cygb/STAP and transgelin synthesis and metalloproteinase 2 activity. Halofuginone increased c-Jun N-terminal kinase phosphorylation in PSCs derived from cerulein-treated mice. Halofuginone prevented the increase in acinar cell proliferation and further increased the cerulein-dependent PAP-1 synthesis.

Conclusions: Halofuginone inhibits Smad3 phosphorylation and increases c-Jun N-terminal kinase phosphorylation, leading to the inhibition of PSC activation and consequent prevention of fibrosis. Halofuginone increased the synthesis of PAP-1, which further reduces pancreas fibrosis. Thus, halofuginone might serve as a novel therapy for pancreas fibrosis.

Key Words: myofibroblasts, pancreatic stellate cells, Smad, collagen, transgelin, cytoglobin

(*Pancreas* 2009;38: 427–435)

Chronic pancreatitis is a progressive disease, characterized by inflammation, fibrosis, and atrophy of the gland tissue, which results in impaired exocrine and endocrine functions of the pancreas.[1] The cellular mechanisms governing pancreas fibrosis are shared among the various insults and, in many aspects, mirror the scarring and wound-healing processes of other tissues. Pancreas fibrosis, regardless of the cause, is characterized by an increase in extracellular matrix (ECM) constituents, although their relative distribution within the pancreas varies with the site and nature of the insult.[2] In the injured pancreas, the pancreatic stellate cells (PSCs) constitute the major source of ECM proteins.[3] These cells are usually quiescent, with a low proliferation rate; however, upon activation, they differentiate into myofibroblastlike cells with high proliferative capacity. The activated PSCs migrate to sites of tissue damage, where they synthesize ECM components to promote tissue repair.[4] The intracellular signaling mechanisms regulating PSC activation include the mitogen-activated protein kinase (MAPK) pathway, which plays a major role in ethanol- and acetaldehyde-dependent activation of PSC, phosphatidylinositol-3-kinase, and protein kinase C.[5]

The transition to the myofibroblastlike phenotype is associated with increased expression of specific smooth muscle genes such as α smooth muscle actin and transgelin (SM22α) and of specific markers such as cytoglobin/stellate cell activation–associated protein (Cygb/STAP) in fibrotic lesions of the pancreas.[6] Pancreatic stellate cells can be activated directly by alcohol consumption[7] or by cytokines derived from the immigrating inflammatory cells.[8,9] Platelet-derived growth factor is the major promoter of PSC migration, whereas transforming growth factor β (TGFβ) affects ECM production via a Smad-associated pathway. Upon phosphorylation by the TGFβ receptor, Smad3 enters the nucleus to modulate the transcription of target genes.[10] Smad3 links TGFβ signaling directly to the serum response factor (SRF)–associated regulatory network that controls the expression of smooth muscle–specific genes.[11,12] The predominant ECM protein synthesized by the PSCs is collagen type I, although increases in the gene expression of other types of collagens and other matrix proteins have also been reported.[13] Pancreas fibrosis may also result from a relative imbalance between the production and degradation of matrix proteins.[14] The PSCs constitute the source of various matrix metalloproteinases (MMPs) and tissue inhibitors of MMPs (TIMPs), which are necessary for ECM remodeling under the control of TGFβ.[15,16]

In addition to the morbidity and mortality caused by chronic pancreatitis, patients with this disease also have a substantially increased risk of developing pancreatic cancer. The PSCs play a major role in the growth and development of pancreas adenocarcinoma, which has a remarkable fibrotic component regulated by the TGFβ pathway.[4,17,18] The desmoplasia is created by activated PSCs, which are stimulated by the cancer cells, thereby influencing tumor aggressiveness.[19] Given that activated PSCs not only are the principal effector cells in pancreas fibrosis but also play a major role in pancreas carcinoma, it seems that targeting the fibroblast-to-PSC transition might be a promising therapeutic approach, for which there is a great unmet need.

From the *Institute of Animal Sciences, The Volcani Center, Bet Dagan, Israel; †Department of Hepatology, Graduate School of Medicine, Osaka City University, Japan; ‡Developmental Biology Laboratory, CLUSTER Project, and 21st Century COE Program, Department of Biological Science, Graduate School of Science, Hiroshima University, Japan; §Department of Animal Sciences, The Hebrew University of Jerusalem, Rehovot, Israel; ||Department of Hematology and Bone Marrow Transplantation, Chaim Sheba Medical Center, Tel Hashomer, Israel; and ¶INSERM U624, Stress Cellulaire, Campus de Luminy, Marseille, France.

Received for publication July 23, 2008; accepted November 24, 2008.

Reprints: Mark Pines, PhD, Institute of Animal Science, ARO, The Volcani Center, Bet Dagan 50250, Israel (e-mail: pines@agri.huji.ac.il).

Halofuginone, an analog of the plant alkaloid febrifugine, has been found to inhibit the activation of hepatic stellate cells (HSCs)[20,21] and the stromal fibroblast-to-myofibroblast transition in the tumor microenvironment.[22] Halofuginone overcame TGFβ-induced collagen synthesis by inhibiting Smad3 phosphorylation downstream of the TGFβ signaling pathway.[23] In animal models in which excess collagen is the hallmark of the disease, halofuginone prevented the increase in collagen synthesis. These models included mice afflicted with chronic graft-versus-host disease and tight-skin mice, rats with pulmonary fibrosis, and rats that developed adhesions at various sites.[23–25] When given to rats that exhibited established fibrosis, halofuginone caused almost a complete resolution of the fibrotic condition.[20] In addition, halofuginone markedly improved the capacity of a cirrhotic liver to regenerate after partial hepatectomy[26] by affecting the expression of early genes of liver regeneration under the control of TGFβ.[27,28] Topical treatment with halofuginone of a patient with chronic graft-versus-host disease and of patients with scleroderma elicited a transient attenuation of collagen α_1(I) gene expression and improvements in skin scores, thus demonstrating human clinical efficacy.[25,29]

In the present study, we evaluated the efficacy of halofuginone in inhibiting pancreas fibrosis in mice, with particular emphasis on TGFβ-dependent PSC activation and ECM production.

MATERIALS AND METHODS

Materials

Halofuginone bromhydrate was obtained from Collgard Biopharmaceuticals Ltd (Tel Aviv, Israel). Cerulein and β-casein were from Sigma (St Louis, Mo). Antibodies to Cygb/STAP were prepared according to Nakatani et al.[6] Smad3 and phosphorylated Smad3 (P-Smad3) antibodies were from Abcam (Cambridge, United Kingdom). Serum response factor antibodies were from Santa Cruz Biotechnology Inc (Santa Cruz, Calif). The proliferating cell nuclear antigen (PCNA) staining kit was from Zymed Laboratories (San Francisco, Calif). Metalloproteinase 2 and P4Hβ monoclonal antibodies were from Acris (Hiddenhausen, Germany), and TIMP1 and TIMP2 monoclonal antibodies were from Lab Vision (Fremont, Calif). Polyclonal antibodies to phospho-Akt (S^{473}P-AKT), phospho-ERK/MAPK (P-p44), total Akt and total ERK/MAPK (p44), and monoclonal antibody to total c-Jun N-terminal kinase (JNK) 1 were from Cell Signaling Technologies (Danvers, Mass). Active-JNK (P-JNK1) and active p38 (P-p38) antibodies were from Promega (Madison, Wis). Rabbit polyclonal antibodies against human pancreatitis-associated protein 1 (PAP-1) were prepared as described previously.[30]

Animal Model of Pancreas Fibrosis

Male ICR mice (Harlan Laboratories, Jerusalem, Israel) were kept under standard conditions with free access to water and chow. Fibrosis was induced in mice (n = 10) by repeated (every 6 h) intraperitoneal injections of cerulein (50 μg/kg) twice weekly for 4 or 8 weeks according to Neuschwander-Tetri et al.[31] Halofuginone was administered intraperitoneally to mice (n = 10) at 4 μg per animal, 3 times per week as described by Bruck et al,[20] starting at the same time as the cerulein. Untreated mice (n = 10) and mice treated only with halofuginone (n = 10) were used as controls. All animal experiments were carried out according to the guidelines of the Volcani Center Institutional Committee for Care and Use of Laboratory Animals (Bet Dagan, Israel).

Preparation of Sections, In Situ Hybridization, and Immunohistochemistry

Pancreas samples were fixed overnight in 4% paraformaldehyde in phosphate-buffered saline at 4°C. Serial 5-μm sections were prepared after the samples had been embedded in Paraplast (McCormick Scientific, St Louis, Mo). Collagenous and noncollagenous proteins were differentially stained with 0.1% Sirius red and 0.1% Fast green as a counterstain, in saturated picric acid. By this procedure, collagen is stained red. Collagen levels were quantified by image analysis (ImagePro; Media Cybernetics, Silver Spring, Md). At least 20 photographs were taken for each analysis per each treatment at each time point. The results were calculated as the red area divided by the total red and green area and presented as arbitrary units of the mean (SE). Special care was taken to exclude the blank areas, which probably represented artifacts. In situ hybridization with a digoxigenin-labeled collagen α_1(I) probe was performed as described by Bruck et al.[20] No signal was observed with the sense probe. For immunohistochemistry, the following antibodies were used: SRF (diluted 1:500), TGFβ1 (1:400), Cygb/STAP (1:700), Smad3 (1:200), P-Smad2/3 (1:700), P4Hβ (1:25), TIMP1 (1:50), TIMP2 (1:250), and PAP-1 (1:10). In all cases, at least 5 slides from all the animals within the group were evaluated blindly to the animal grouping.

Cell Culture

Pancreatic stellate cells were prepared from either control mice or mice treated with a single injection of cerulein (50 μg/kg). After 24 hours, the pancreas was excised, freed from fat and lymph nodes, and digested with collagenase IV (0.02%), and the resulting cell suspension was centrifuged at 1200*g* for 5 minutes. The cells were washed and resuspended in Dulbecco's modified essential medium (DMEM) containing 10% fetal bovine serum and antibiotics (100-U/mL penicillin, 100-mg/mL streptomycin) and plated on 6-well plates with the same medium.[32] No significant differences were observed in the cell yield between the control and cerulein-treated mice, and almost all the cells were stained positive for Cygb/STAP or SM22α. All of the cells were incubated at 37°C in a humidified atmosphere containing 5% carbon dioxide. The cells were incubated with serum-free DMEM for 6 hours and were then treated with fresh medium containing halofuginone (20 or 50 nmol/L), TGFβ (3 ng/mL), or both for an additional 24 hours. Cellular viability was determined by trypan blue exclusion. At the end of the incubation period, the cells were either counted directly with a cell counter (Coulter Electronics, Bath, United Kingdom) or resuspended in 500 μL of lysis buffer consisting of 1-mmol/L EDTA, 50-mmol/L Tris (pH, 7.5), 150-mmol/L NaCl, 10% glycerol, 1% Nonidet P40, and a 1:100 dilution of protease and phosphatase inhibitor cocktail (Sigma).

Western Blot

Protein lysate (30 μg) from either tissue or cells was electrophoresed on a 10% sodium dodecyl sulfate–polyacrylamide gel and transferred onto a nitrocellulose membrane. Nonspecific binding sites were blocked with 5% low-fat milk, and the membranes were incubated overnight with the appropriate antibodies for SM22α (1:5000), Cygb/STAP (1:1000), MMP-2 (1:200), phospho-Akt (1:1000), phosphor-ERK/MAPK (1:2000), total Akt and total ERK/MAPK (1:1500), active

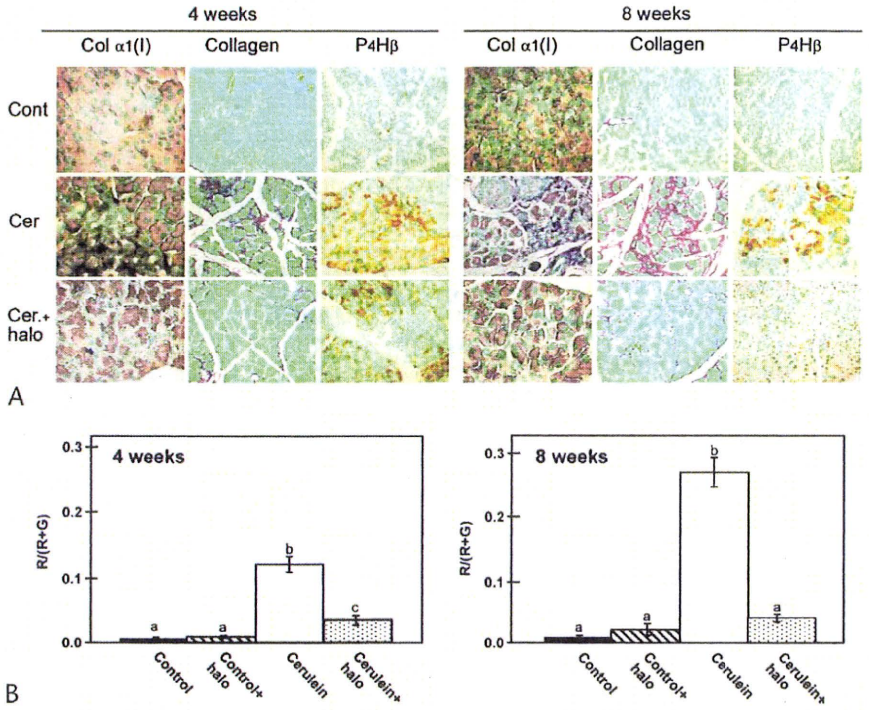

FIGURE 1. Effect of halofuginone on cerulein-dependent synthesis of collagen and P4Hβ, a collagen cross-linking enzyme. Mice were treated with cerulein for 4 or 8 weeks with or without halofuginone, after which pancreas biopsies were taken for histology. A, Collagen α_1(I) gene expression was determined by in situ hybridization, collagen level was evaluated by Sirius red staining, and P4Hβ was determined by immunohistochemistry. B, Image analysis of pancreas collagen levels. In each column, means without a common letter differ significantly ($P < 0.05$) according to Duncan multiple range test.

JNK (1:5000), active p38 (1:2000), and monoclonal antibody to total JNK (1:1000).

Zymography

Conditioned medium samples were analyzed for MMP activity, which was determined in a 10% sodium dodecyl sulfate–polyacrylamide gel impregnated with gelatin (0.01%) or β-casein (1.0 mg/mL). Proteins were separated on the gel under nonreducing conditions, followed by 1 hour of incubation in 2.5% Triton X-100 and 16 hours of incubation in 50-mmol/L Tris (pH, 7.6), 0.2-mol/L NaCl, and 5-mmol/L $CaCl_2$ at 37°C. After the incubation period, the gels were stained with 0.5% Coomassie G 250 in methanol/acetic acid/water (30:10:60, vol/vol/vol).

Statistical Analysis

The results are presented as the mean (SD). The significance of differences among different groups was determined by analysis of variance. In each column, means without a common letter differ significantly ($P < 0.05$) according to Duncan multiple range test.

RESULTS

Halofuginone Inhibits Pancreas Fibrosis

Pancreas fibrosis is the result of a dynamic cascade of mechanisms beginning with acinar cell injury and followed by inflammation and PSC activation. After 4 weeks of cerulein treatment, we observed a major increase in the number of PSCs expressing the collagen α_1(I) gene, the synthesis of large quantities of collagen surrounding the acinar cells, and positive staining for P4Hβ, one of the major enzymes responsible for collagen cross-linking and maturation (Fig. 1A). Collagen accumulated in the pancreas with time, and after an additional 4 weeks of cerulein treatment, a further increase in collagen content and P4Hβ level was observed. Halofuginone prevented the increase in fibrosis in a time-dependent fashion, as demonstrated by reductions in the expression of the collagen α_1(I) gene, in collagen content, and in the level of P4Hβ. After 4 weeks of halofuginone treatment, the collagen level was significantly lower than that of the cerulein-treated mice but was still higher than that of the control mice. After 8 weeks of halofuginone treatment, the collagen level was significantly lower than that of the cerulein-treated mice and did not differ from that of the control untreated mice (Fig. 1B). Halofuginone alone had no effect on the collagen content or other histologic parameters in the control untreated mice (data not shown).

Halofuginone Inhibits PSC Activation

In addition to enhancing collagen synthesis, activated PSCs are also characterized by increased proliferation and expression of SM22α and Cygb/STAP genes under the control of TGFβ. After 4 weeks of cerulein treatment, a major increase in the number of PSCs exhibiting Cygb/STAP was observed, which persisted for at least 8 weeks. Halofuginone reduced the number of Cygb/STAP-positive cells in the pancreas (Fig. 2A) and inhibited the TGFβ-induced Cygb/STAP levels in primary PSCs in cultures derived from the pancreas of control and cerulein-treated mice (Fig. 2B). Transgelin is induced during transdifferentiation of fibroblasts to myofibroblasts at the time of stromal tissue remodeling under the

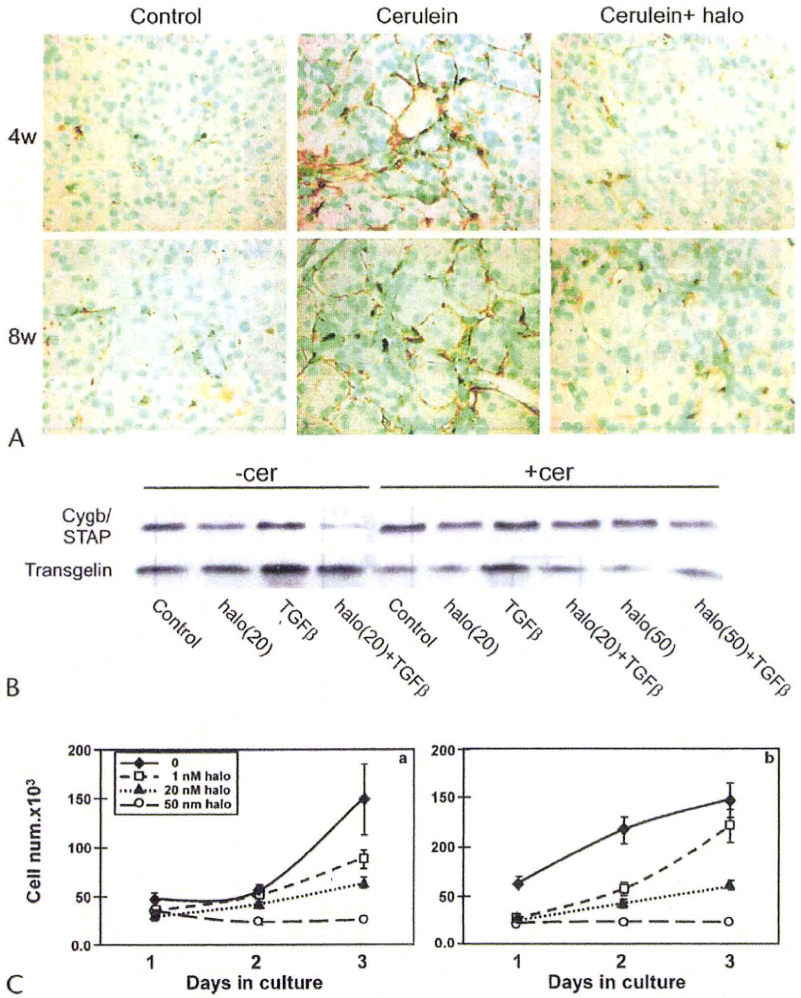

FIGURE 2. Effect of halofuginone on the synthesis of Cygb/STAP and SM22α and on PSC proliferation. A, Immunohistochemistry of Cygb/STAP in pancreas biopsies of mice treated for 4 or 8 weeks with cerulein, with or without halofuginone. B, Western blotting of Cygb/STAP and SM22α of PSCs derived from either control or cerulein-treated mice. The cells were incubated for 18 hours with TGFβ (3 ng/mL), halofuginone, or their combination. C, Primary PSCs were incubated with various concentrations of halofuginone, and cell proliferation was estimated directly by cell counting.

control of TGFβ. The PSCs in culture from control and cerulein-treated mice synthesized SM22α, which was upregulated by TGFβ. Halofuginone prevented the TGFβ-dependent SM22α synthesis in cultured primary PSCs derived from either control or cerulein-treated mice (Fig. 2B). The inhibitory effect of halofuginone on Cygb/STAP and SM22α synthesis was accompanied by a dose-dependent inhibition of proliferation of PSCs derived from either the normal pancreas or cerulein-treated mice (Fig. 2C). All of these findings were consistent with halofuginone inhibition of PSC activation.

Halofuginone and Matrix Degradation

The levels of TIMP1 and TIMP2 were increased in the pancreas after cerulein treatment, but only the TIMP2 level was inhibited by halofuginone (Fig. 3A). Metalloproteinase 2 is one of the major MMPs involved in pancreas fibrosis under the control of TGFβ.[14–16] Halofuginone had only a minimal, if any, effect on MMP-2 levels in the control mice. Cerulein treatment caused an increase in MMP-2 levels, which were further increased after halofuginone treatment (Fig. 3B). In culture, a major increase in basal MMP-2 activity was observed in conditioned medium of PSCs derived from cerulein-treated mice compared with controls (Fig. 3C). Halofuginone had no effect on the basal level of MMP-2 activity but inhibited the TGFβ-dependent increase in its activity by PSCs derived from control and cerulein-treated mice (Fig. 3D). In contrast, halofuginone increased MMP-3 activity, but only in PSCs derived from cerulein-treated mice (Fig. 3E).

Halofuginone Inhibits TGFβ Signaling

Almost no TGFβ was observed in the control untreated pancreas, whereas in the cerulein-treated mice, a major increase in its level was observed, mostly in the acinar cells but also in some of the PSCs (Fig. 4). Halofuginone treatment did not cause any change in the level of TGFβ, in agreement with previous studies suggesting that halofuginone affects TGFβ signaling downstream in its pathway.[23] Halofuginone treatment eliminated the synthesis of SRF, which was observed exclusively in the PSCs of the cerulein-treated pancreas. In the untreated pancreas, Smad3 was observed only in endothelial cells

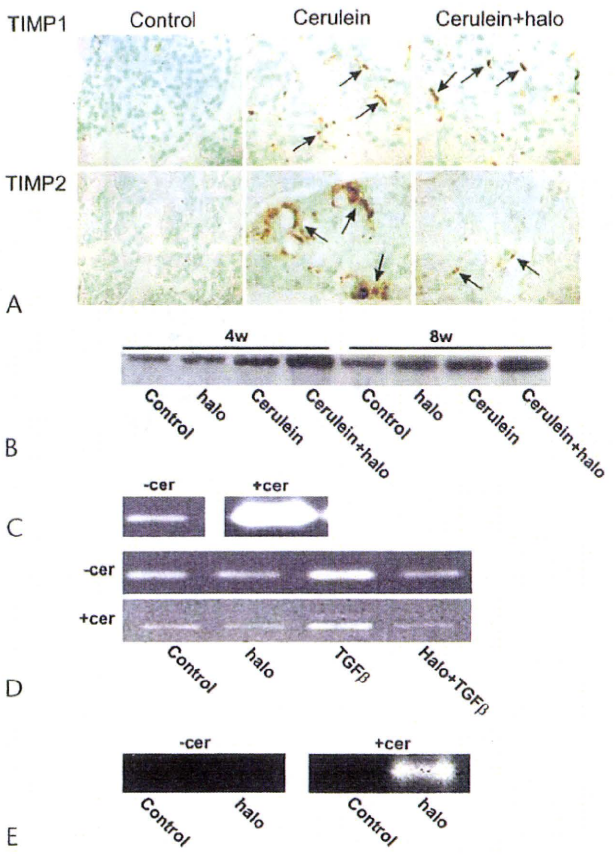

FIGURE 3. Halofuginone and the ECM degradation pathway. A, Immunohistochemistry of TIMP1 and TIMP2 in the pancreas after 8 weeks of cerulein treatment, with or without halofuginone. B, Western blotting with MMP-2 antibodies of pancreas extracts. C, Gelatin zymography for evaluation of MMP-2 activity in conditioned medium of PSCs derived from the cerulein-treated or untreated pancreas. Note the high levels of MMP-2 activity in conditioned medium of PSCs derived from the cerulein-treated pancreas. D, Effect of halofuginone on MMP-2 activity. E, Metalloproteinase 3 in conditioned medium collected from PSCs derived from the normal and the cerulein-treated pancreas.

surrounding the blood vessels, and no P-Smad3 was observed in any cell type. After cerulein treatment, increases in Smad3 and P-Smad3 were observed. Smad3 was observed mostly in the PSCs, whereas P-Smad3 was observed in the acinar cells and the PSCs. Halofuginone had no effect on the level of Smad3 protein expression, whereas complete elimination of P-Smad3 was observed after halofuginone treatment (Fig. 4).

Intracellular PSC Signaling Is Affected by Halofuginone

We evaluated the effect of halofuginone on the phosphorylation of key proteins in the MAPK pathways—JNK, MAPK/ERK, and p38 MAPK—and on Akt in PSCs derived from the control and the cerulein-treated pancreas (Fig. 5). Levels of phosphorylated JNK and, to a much lesser extent, phosphorylated MAPK/ERK were higher in the PSCs derived from the cerulein-treated pancreas relative to controls and were further increased after halofuginone treatment. Equal levels of phosphorylated Akt and p38 MAPK were observed in PSCs derived from control and cerulein-treated mice and were unaltered after halofuginone treatment.

Halofuginone Affects Cerulein-Dependent Acinar Cell Proliferation and PAP-1 Synthesis

Fully differentiated pancreatic acinar cells are capable of replication and can reenter the cell cycle to restore lost acinar tissue.[44] Only a small number of PCNA-positive acinar cells were detected in the untreated pancreas, whereas after cerulein treatment, a major increase in PCNA-positive cells was observed (Fig. 6). Halofuginone prevented this increase only in the early stages of pancreas fibrosis development. In pathologic situations, the acinar cells are the main source of PAP-1.[33] Almost no PAP-1 was synthesized by the control untreated pancreas or by the pancreas of mice treated with halofuginone alone. Cerulein caused increased PAP-1 synthesis, which was more evident after 4 weeks of treatment, and halofuginone caused a further increase in this synthesis (Fig. 7).

DISCUSSION

Chronic pancreatitis is characterized by pancreatic inflammation and fibrosis, eventually leading to destruction of pancreatic parenchyma and loss of exocrine and endocrine functions. In response to pancreatic injury or inflammation, PSCs are activated into highly proliferative myofibroblastlike cells that express smooth muscle proteins and produce ECM components. Administration of cerulein caused a major increase in the synthesis of fibrosis-related and TGFβ-dependent proteins such as collagen type I and P4Hβ (Fig. 1), consistent with other models of pancreatitis.[34,35] Halofuginone inhibited PSC activation, in agreement with previous observations of inhibition of HSC and tumor myofibroblast activation,[20,22,23] as evidenced by the following findings. (1) There was inhibition of synthesis of collagen type I, the major ECM protein, and of P4Hβ, the main enzyme responsible for its cross-linking (Fig. 1). The Sirius red staining that remained after halofuginone treatment may partly represent collagen type III, which also increases in pancreas fibrosis[35] but is not affected by halofuginone.[36] Halofuginone also inhibited collagen synthesis in severe hyperstimulation and obstruction pancreatitis in rats.[37] (2) There was inhibition of the expression of specific markers expressed in activated PSCs, such as Cygb/STAP, and of TGFβ-dependent increases in muscle-specific genes such as SM22α (Figs. 2A, B). (3) There was inhibition of PSC proliferation (Fig. 2C). All of the inhibited parameters are characteristic of activated PSCs. Transforming growth factor β is known to regulate PSC activation and to inhibit its proliferation. Although halofuginone inhibited TGFβ signaling, incubation of the PSC with halofuginone resulted in a dose-dependent inhibition of cell proliferation (Fig. 2C). These results suggest that halofuginone may have additional targets involved in cell proliferation, for example, within the MAPK signaling pathway (Fig. 5).

The course of chronic pancreatitis is characterized by recurrent episodes of acute pancreatitis, which cause parenchymal injury and necrosis, accompanied by fibrosis, chronic inflammation, and parenchymal cell loss, all of which increase with each successive episode. Hypoxia and hypoxia-related genes are upregulated during cerulein-induced acute pancreatitis.[38] It is interesting to note that the synthesis of Cygb/STAP and collagen P4Hβ is controlled by hypoxia.[39,40] Cytoglobin/stellate cell activation–associated protein is probably involved in cellular oxygen homeostasis and supply and plays a role as an oxygen reservoir that is used under hypoxic conditions to protect the tissue from oxidative stress.[41]

Regardless of the cause of the insult resulting in pancreas fibrosis, extensive ECM remodeling is required. In the first

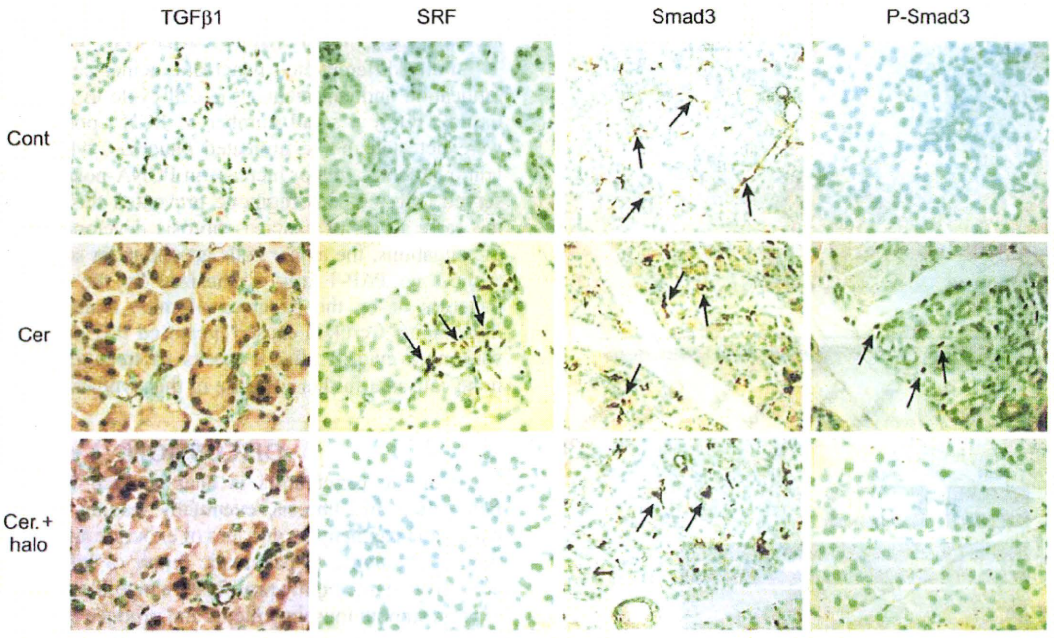

FIGURE 4. Halofuginone and TGFβ signaling. Transforming growth factor β, SRF, Smad3, and P-Smad3 levels were determined by immunohistochemistry in pancreas biopsies after 8 weeks of cerulein treatment, with or without halofuginone. Cells expressing the specific proteins are indicated by arrows. Note that halofuginone did not affect TGFβ levels but prevented the cerulein-dependent increases in SRF and P-Smad3, but not Smad3, levels.

step, transient local degradation of the ECM occurs, either by proteases of the plasminogen or by the MMP systems. The balance between the MMPs and their inhibitors is pivotal in the remodeling of the ECM. Tissue inhibitors of MMP-1 and TIMP2, derived from the activated PSCs,[16] are increased in the pancreas of cerulein-treated mice (Fig. 3A). Although both TIMPs are under the control of TGFβ, the regulation of TIMP1 is probably not Smad3-dependent. The Smad-containing complexes do not interact with the promoter-proximal activator protein 1 site of TIMP1 that is required for TGFβ activation; therefore, TGFβ was able to stimulate TIMP1 synthesis in a Smad-knockout cell line.[42] This could explain the observation that halofuginone, an inhibitor of Smad3 phosphorylation downstream of TGFβ signaling[21,23] (Fig. 4), inhibited only the synthesis of TIMP2 but not that of TIMP1 (Fig. 3A), as has been observed in chemically induced liver fibrosis.[20] Pancreatic stellate cells have the capacity to synthesize a number of MMPs under the control of TGFβ.[16] The PSCs derived from cerulein-treated mice exhibited much higher MMP-2 activity than those derived from the control mice, and the difference persisted even after several passages in culture (Fig. 3C). This may imply a fundamental genomic change while they are in the fibrotic tissue, or it may reflect the disparity in their origin. Halofuginone prevented the TGFβ-dependent increase in MMP-2 activity in both cell populations (Fig. 3D), but it increased MMP-3 activity only in the cells derived from cerulein-treated mice. These results are consistent with the effects of halofuginone on MMP activity observed in HSCs in culture and in rat hepatic-induced fibrosis.[43]

Transforming growth factor β is synthesized by the PSCs and was upregulated in the cerulein-treated pancreas (Fig. 4). Halofuginone, which has been found to overcome TGFβ-induced collagen synthesis without affecting TGFβ receptor expression,[23] did not affect TGFβ levels in the cerulein-treated mice, suggesting that halofuginone's target is probably downstream of the TGFβ-receptor interaction, along the Smad3 pathway. Indeed, halofuginone decreased the levels of P-Smad2/3 in the cerulein-treated pancreas without affecting the total level of Smad3, in agreement with previous findings.[21,23] Smad3, in conjunction with SRF, is a major mediator of TGFβ signaling, which results in transcription of smooth muscle–specific genes.[11] Serum response factor induces smooth muscle cell (SMC) gene expression, and the dominant-negative mutant of SRF blocks TGFβ-induced SMC genes.[44] In activated HSCs, TGFβ upregulates SRF synthesis, resulting in SMC gene expression.[45] The entire conditional inactivation of the SRF gene in the pancreas leads to severe pancreatitis,[46] although in the present study, in the cerulein-treated pancreas, SRF was upregulated exclusively by the PSCs, probably because of cerulein-dependent increases in TGFβ synthesis and Smad3 phosphorylation (Fig. 4). Halofuginone inhibited SRF synthesis without affecting the level of TGFβ, which again suggests that halofuginone inhibits smooth muscle gene expression and ECM production by inhibiting Smad3 phosphorylation downstream of TGFβ signaling, resulting in inhibition of PSC activation.

The PSCs derived from the pancreas of cerulein-treated mice exhibited much higher levels of phosphorylated JNK and, to a lesser extent, of MAPK/ERK, but not of p38 kinase or Akt. Halofuginone further increased JNK phosphorylation in the cerulein-treated PSCs. The JNK has been implicated as a repressor of TGFβ gene expression, and it contributes to the regulation of autocrine TGFβ-mediated biologic responses,[47] suggesting that there is cross-talk between the 2 signaling pathways. It is interesting to note that halofuginone causes increased phosphorylation of c-Jun transcription factor, a major JNK substrate, in Tsk/+ mouse fibroblasts in culture and in vivo, in correlation with a decrease in collagen synthesis.[48]

Halofuginone affects not only the stellate cells but also the epithelial cells of the tissue. In the liver, halofuginone stimulates insulin growth factor binding protein 1 synthesis by the hepatocytes, and the secreted insulin growth factor binding

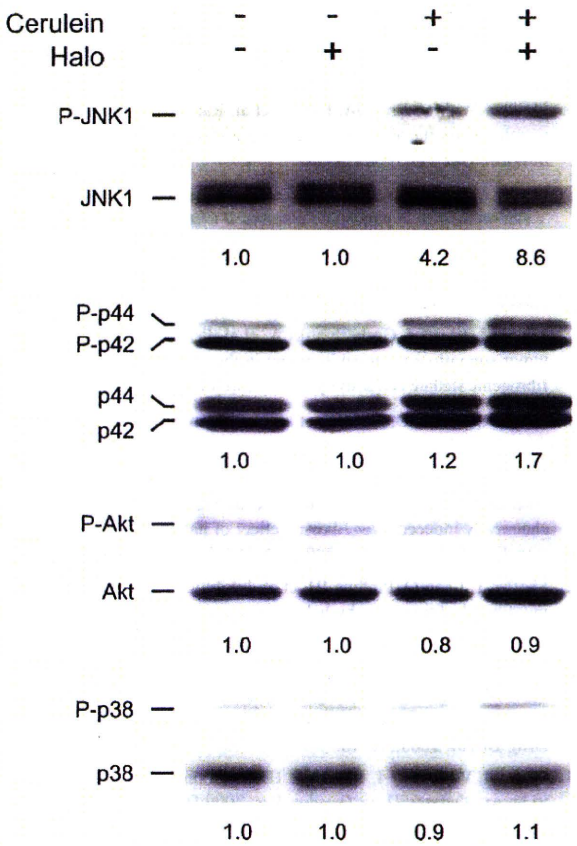

FIGURE 5. Halofuginone and JNK, MAPK, and Akt signaling in PSCs. Cells derived from the pancreas of control and cerulein-treated mice were cultured in the presence or absence of halofuginone (20 mmol/L). At the end of the incubation, cell extracts were blotted with the appropriate antibodies. Halofuginone further increased the cerulein-dependent phosphorylation of JNK and, to a lesser extent, the phosphorylation of MAPK/ERK. No effect of cerulein or halofuginone on Akt or p38 phosphorylation was observed.

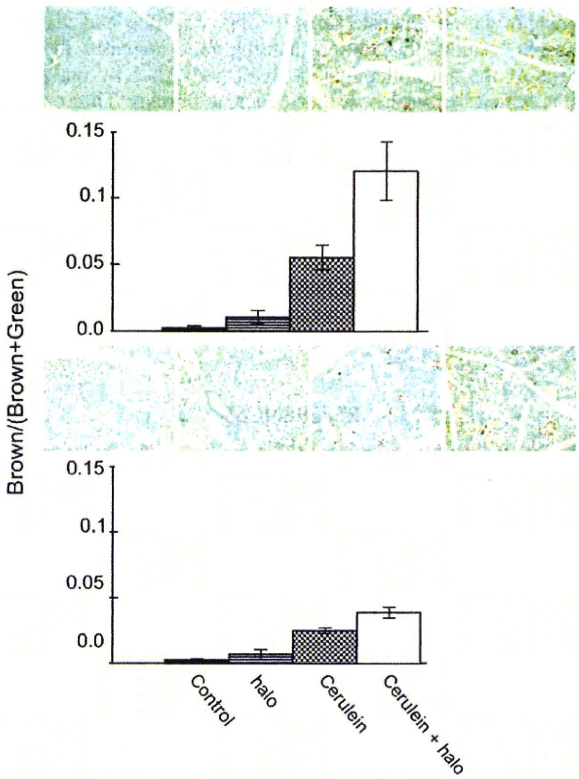

FIGURE 7. Halofuginone and PAP-1 synthesis. Pancreas biopsies were taken after 4 and 8 weeks of cerulein treatment, with and without halofuginone, immunostained with PAP-1 antibodies, and subjected to image analysis. In each panel, means without a common letter differ significantly ($P < 0.05$) according to Duncan multiple range test.

protein 1 inhibits HSC migration.[27] In the pancreas, PAP-1 is expressed at a level related to the severity of cerulein-induced pancreatitis in the acute phase.[49] Halofuginone prevented the cerulein-dependent increase in acinar cell proliferation and increased the synthesis of anti-inflammatory cytokine PAP-1 (Figs. 6, 7), which may further reduce PSC activation and matrix synthesis, by inhibiting inflammation. Halofuginone also inhibited rat inflammation after severe hyperstimulation and obstruction pancreatitis.[37]

In conclusion, we demonstrated that halofuginone prevents cerulein-dependent PSC activation by inhibiting Smad3

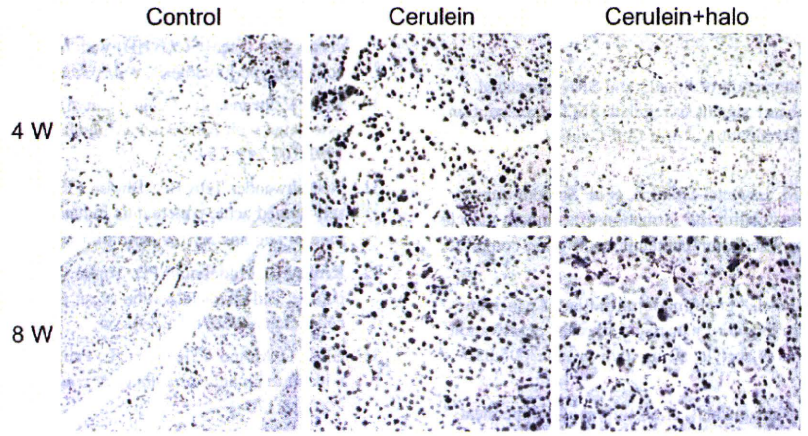

FIGURE 6. Halofuginone and acinar cell proliferation. Pancreas biopsies were taken after 4 and 8 weeks of cerulein treatment, with and without halofuginone, and were immunostained with PCNA antibodies. Halofuginone prevented the increase in acinar cell proliferation after only 4 weeks of treatment.

phosphorylation downstream of TGFβ signaling and via JNK phosphorylation. In addition, halofuginone increases the synthesis of the anti-inflammatory cytokine PAP-1 by the acinar cells, which can further reduce pancreas fibrosis. These results suggest that halofuginone, which has already exhibited human clinical efficacy[25,29] and is currently being evaluated in clinical trials for various indications,[50] could serve as a novel therapy for pancreas fibrosis.

ACKNOWLEDGMENT

This article is a contribution from the ARO, The Volcani Center.

REFERENCES

1. Witt H, Apte MV, Keim V, et al. Chronic pancreatitis: challenges and advances in pathogenesis, genetics, diagnosis, and therapy. *Gastroenterology*. 2007;132:1557–1573.
2. Kloppel G, Detlefsen S, Feyerabend B. Fibrosis of the pancreas: the initial tissue damage and the resulting pattern. *Virchows Arch*. 2004;445:1–8.
3. Apte MV, Wilson JS. Mechanisms of pancreatic fibrosis. *Dig Dis*. 2004;22:273–279.
4. Bachem MG, Schunemann M, Ramadani M, et al. Pancreatic carcinoma cells induce fibrosis by stimulating proliferation and matrix synthesis of stellate cells. *Gastroenterology*. 2005;128:907–921.
5. McCarroll JA, Phillips PA, Park S, et al. Pancreatic stellate cell activation by ethanol and acetaldehyde: is it mediated by the mitogen-activated protein kinase signaling pathway? *Pancreas*. 2003;27:150–160.
6. Nakatani K, Okuyama H, Shimahara Y, et al. Cytoglobin/STAP, its unique localization in splanchnic fibroblast-like cells and function in organ fibrogenesis. *Lab Invest*. 2004;84:91–101.
7. Apte MV, Phillips PA, Fahmy RG, et al. Does alcohol directly stimulate pancreatic fibrogenesis? Studies with rat pancreatic stellate cells. *Gastroenterology*. 2000;118:780–794.
8. Luttenberger T, Schmid-Kotsas A, Menke A, et al. Platelet-derived growth factors stimulate proliferation and extracellular matrix synthesis of pancreatic stellate cells: implications in pathogenesis of pancreas fibrosis. *Lab Invest*. 2000;80:47–55.
9. Yoo BM, Yeo M, Oh TY, et al. Amelioration of pancreatic fibrosis in mice with defective TGF-beta signaling. *Pancreas*. 1995;30:71–79.
10. Roberts AB, Russo A, Felici A, et al. Smad3: a key player in pathogenetic mechanisms dependent on TGF-beta. *Ann N Y Acad Sci*. 2003;995:1–10.
11. Qiu P, Feng XH, Li L. Interaction of Smad3 and SRF-associated complex mediates TGF-beta1 signals to regulate SM22 transcription during myofibroblast differentiation. *J Mol Cell Cardiol*. 2003;35:1407–1420.
12. Mack CP, Thompson MM, Lawrenz-Smith S, et al. Smooth muscle alpha-actin CArG elements coordinate formation of a smooth muscle cell–selective, serum response factor–containing activation complex. *Circ Res*. 2000;86:221–232.
13. Jesnowski R, Furst D, Ringel J, et al. Immortalization of pancreatic stellate cells as an in vitro model of pancreatic fibrosis: deactivation is induced by matrigel and *N*-acetylcysteine. *Lab Invest*. 2005;85:1276–1291.
14. Ishihara T, Hayasaka A, Yamaguchi T, et al. Immunohistochemical study of transforming growth factor-beta 1, matrix metalloproteinase-2,9, tissue inhibitors of metalloproteinase-1,2, and basement membrane components at pancreatic ducts in chronic pancreatitis. *Pancreas*. 1998;17:412–418.
15. Yokota T, Denham W, Murayama K, et al. Pancreatic stellate cell activation and MMP production in experimental pancreatic fibrosis. *J Surg Res*. 2002;104:106–111.
16. Phillips PA, McCarroll JA, Park S, et al. Rat pancreatic stellate cells secrete matrix metalloproteinases: implications for extracellular matrix turnover. *Gut*. 2003;52:275–282.
17. Omary MB, Lugea A, Lowe AW, et al. The pancreatic stellate cell: a star on the rise in pancreatic diseases. *J Clin Invest*. 2007;117:50–59.
18. Hwang RF, Moore T, Arumugam T, et al. Cancer-associated stromal fibroblasts promote pancreatic tumor progression. *Cancer Res*. 2008;68:918–926.
19. Erkan M, Kleeff J, Gorbachevski A, et al. Periostin creates a tumor-supportive microenvironment in the pancreas by sustaining fibrogenic stellate cell activity. *Gastroenterology*. 2007;132:1447–1464.
20. Bruck R, Genina O, Aeed H, et al. Halofuginone to prevent and treat thioacetamide-induced liver fibrosis in rats. *Hepatology*. 2001;3:379–386.
21. Gnainsky Y, Kushnirsky Z, Bilu G, et al. Gene expression during chemically induced liver fibrosis: effect of halofuginone on TGF-beta signaling. *Cell Tissue Res*. 2007;328:153–166.
22. Sheffer Y, Leon O, Pinthus JH, et al. Inhibition of fibroblast to myofibroblast transition by halofuginone contributes to the chemotherapy-mediated antitumoral effect. *Mol Cancer Ther*. 2007;6:570–577.
23. Pines M. Targeting TGFβ signaling to inhibit fibroblast activation as a therapy for fibrosis and cancer: effect of halofuginone. *Exp Opion Drug Discov*. 2008;3:1–10.
24. Pines M, Vlodavsky I, Nagler A. Halofuginone: from veterinary use to human therapy. *Drug Develop Res*. 2000;50:371–378.
25. Pines M, Snyder D, Yarkoni S, et al. Halofuginone to treat fibrosis in chronic graft versus host disease and scleroderma. *Biol Bl Marrow Transplant*. 2003;9:417–425.
26. Spira G, Mawasi N, Paizi M, et al. Halofuginone, a collagen type I inhibitor improves liver regeneration in cirrhotic rats. *J Hepatol*. 2002;37:331–339.
27. Gnainsky Y, Spira G, Paizi M, et al. Halofuginone—an inhibitor of collagen synthesis by rat stellate cells—stimulates insulin-like growth factor-binding protein 1 synthesis by hepatocytes. *J Hepatol*. 2003;40:269–277.
28. Gnainsky Y, Spira G, Paizi M, et al. The involvement of the tyrosine phosphatase early gene of liver regeneration (PRL-1) in cell cycle and in liver regeneration and fibrosis—effect of halofuginone. *Cell Tissue Res*. 2006;324:385–394.
29. Nagler A, Pines M. Topical treatment of cutaneous chronic graft versus host disease (cGvHD) with halofuginone: a novel inhibitor of collagen type I synthesis. *Transplantation*. 1999;68:1806–1809.
30. Keim V, Iovanna JL, Orelle B, et al. A novel exocrine protein associated with pancreas transplantation in humans. *Gastroenterology*. 1992;103:248–254.
31. Neuschwander-Tetri BA, Burton FR, Presti ME, et al. Repetitive self-limited acute pancreatitis induces pancreatic fibrogenesis in the mouse. *Dig Dis Sci*. 2000;45:665–674.
32. Kruse ML, Hildebrand PB, Timke C, et al. Isolation, long-term culture, and characterization of rat pancreatic fibroblastoid/stellate cells. *Pancreas*. 2001;23:49–54.
33. Closa D, Motoo Y, Iovanna JL. Pancreatitis-associated protein: from a lectin to an anti-inflammatory cytokine. *World J Gastroenterol*. 2007;13:170–174.
34. Koslowski R, Seidel D, Kuhlisch E, et al. Evidence for the involvement of TGF-beta and PDGF in the regulation of prolyl 4-hydroxylase and lysyloxidase in cultured rat lung fibroblasts. *Exp Toxicol Pathol*. 2003;55:257–264.

35. Miyauchi M, Suda K, Kuwayama C, et al. Role of fibrosis-related genes and pancreatic duct obstruction in rat pancreatitis models: implications for chronic pancreatitis. *Histol Histopathol*. 2007;22:1119–1127.

36. Choi ET, Callow AD, Sehgal NL, et al. Halofuginone, a specific collagen type I inhibitor, reduces anastomotic intimal hyperplasia. *Arch Surg*. 1995;130:257–261.

37. Karatas A, Paksoy M, Erzin Y, et al. The effect of halofuginone, a specific inhibitor of collagen type 1 synthesis, in the prevention of pancreatic fibrosis in an experimental model of severe hyperstimulation and obstruction pancreatitis. *J Surg Res*. 2008;148:7–12.

38. Gomez G, Englander EW, Wang G, et al. Increased expression of hypoxia-inducible factor-1alpha, p48, and the Notch signaling cascade during acute pancreatitis in mice. *Pancreas*. 2004;28:58–64.

39. Fähling M, Perlewitz A, Doller A, et al. Regulation of collagen prolyl 4-hydroxylase and matrix metalloproteinases in fibrosarcoma cells by hypoxia. *Comp Biochem Physiol C Toxicol Pharmacol*. 2004;139:119–126.

40. Fordel E, Thijs L, Martinet W, et al. Anoxia or oxygen and glucose deprivation in SH-SY5Y cells: a step closer to the unraveling of neuroglobin and cytoglobin functions. *Gene*. 2007;398:114–122.

41. Xu R, Harrison PM, Chen M, et al. Cytoglobin overexpression protects against damage-induced fibrosis. *Mol Ther*. 2006;13:1093–1100.

42. Hall MC, Young DA, Waters JG, et al. The comparative role of activator protein 1 and Smad factors in the regulation of Timp-1 and MMP-1 gene expression by transforming growth factor-beta 1. *J Biol Chem*. 2003;278:10304–10313.

43. Popov Y, Patsenker E, Bauer M, et al. Halofuginone induces matrix metalloproteinases in rat hepatic stellate cells via activation of p38 and NFkappaB. *J Biol Chem*. 2006;281:15090–15098.

44. Hirschi KK, Lai L, Belaguli NS, et al. Transforming growth factor-beta induction of smooth muscle cell phenotype requires transcriptional and post-transcriptional control of serum response factor. *J Biol Chem*. 2002;277:6287–6295.

45. Herrmann J, Haas U, Gressner AM, et al. TGF-beta up-regulates serum response factor in activated hepatic stellate cells. *Biochim Biophys Acta*. 2007;1772:1250–1257.

46. Miralles F, Hebrard S, Lamotte L, et al. Conditional inactivation of the murine serum response factor in the pancreas leads to severe pancreatitis. *Lab Invest*. 2006;86:1020–1036.

47. Ventura JJ, Kennedy NJ, Flavell RA, et al. JNK regulates autocrine expression of TGF-beta1. *Mol Cell*. 2004;15:269–278.

48. McGaha TL, Kodera T, Spiera H, et al. Halofuginone inhibition of COL1A2 promoter activity via a c-Jun–dependent mechanism. *Arthritis Rheum*. 2002;46:2748–2761.

49. Magaña-Gómez J, López-Cervantes G, Calderón de la Barca AM. Caerulin-induced pancreatitis in rats: histological and genetic expression changes from acute phase to recuperation. *World J Gastroenterol*. 2006;12:3999–4003.

50. de Jonge MJ, Dumez H, Verweij J, et al. EORTC New Drug Development Group (NDDG). Phase I and pharmacokinetic study of halofuginone, an oral quinazolinone derivative in patients with advanced solid tumours. *Eur J Cancer*. 2006;42:1768–1774.

Xenotransplantation 2008: 15: 235–245
Printed in Singapore. All rights reserved
doi: 10.1111/j.1399-3089.2008.00483.x

Engraftment of human hepatocytes in the livers of rats bearing bone marrow reconstructed with immunodeficient mouse bone marrow cells

Igarashi Y, Tateno C, Tanaka Y, Tachibana A, Utoh R, Kataoka M, Ohdan H, Asahara T, Yoshizato K. Engraftment of human hepatocytes in the livers of rats bearing bone marrow reconstructed with immunodeficient mouse bone marrow cells.
Xenotransplantation 2008; 15: 235–245. © 2008 Wiley Periodicals, Inc.

Abstract: Background: Previously, we created, a chimeric mouse (humanized mouse), a severe combined immunodeficiency (SCID) mouse whose liver was >90% repopulated with human (*h*)-hepatocytes, which are useful for the testing of drug metabolism and toxicity, as well as a hepatitis B virus and hepatitis C virus-susceptible animal model. However, their small body size and small total blood volume limited the utilization for analytical purposes, which led us to develop a method to create a chimeric rat bearing *h*-hepatocyte-repopulated liver.
Methods: F344 nude rats devoid of T cells were irradiated with X-rays and injected with bone marrow cells (BMCs) from SCID mice (m_{SCID}). The rate of replacement with m_{SCID}-BMCs was evaluated by two-color flow cytometry analysis of peripheral blood mononuclear cells (PBMCs). After m_{SCID}-BMCs repopulated the host bone marrow (BM), the rats were treated with retrorsine, partially hepatectomized (PHx), and transplanted with 5×10^6 *h*-hepatocytes isolated from the chimeric mice. *h*-Albumin (*h*-Alb) concentrations in the host blood and the expression levels of protein and mRNA of hepatocyte differentiation markers in the *h*-hepatocytes were evaluated by ELISA, immunostaining, and reverse transcription-PCR, respectively.
Results: The m_{SCID}-BMCs successfully repopulated the rats, the percentage of mouse cells reaching 94% among host ($r_{nudeF344}$) PBMCs at 4 weeks after *m*-BMC transplantation. *h*-Hepatocytes isolated from the chimeric mice were transplanted to the liver of the m_{SCID}-BMC-repopulated rats. The engrafted *h*-hepatocytes expressed *h*-Alb and *h*-cytochrome P450 (CYP) subtypes and survived showing normal phenotypes until at least 3 weeks post-*h*-hepatocytes transplantation (*h*-HPCT). However, the blood concentrations of *h*-Alb declined at 4 weeks post-HPCT, concomitant with the emergence of both $r_{nudeF344}$- and m_{SCID}-macrophages, suggesting the rejection of *h*-hepatocytes due to the activation of macrophages.
Conclusion: We developed a novel method to create a rat that bears the liver engrafted with *h*-hepatocytes, utilizing a rat with the BM composed of m_{SCID}-BMCs as a host. This *h*-hepatocyte-bearing rat will be a valuable model for studying the immunologic mechanisms involved in xenogeneic transplantation and for generating rats with higher rates of repopulation with *h*-hepatocytes.

Yuka Igarashi,[1,2] Chise Tateno,[2,*] Yuka Tanaka,[1] Asato Tachibana,[2,3] Rie Utoh,[2,†] Miho Kataoka,[2] Hideki Ohdan,[1] Toshimasa Asahara[1] and Katsutoshi Yoshizato[2,4,*]

[1]Department of Surgery, Division of Frontier Medical Science, Program for Biomedical Research, and Hiroshima University 21st Century COE Program for Advanced Radiation Casualty Medicine, Graduate School of Biomedical Sciences, Hiroshima University, [2]Yoshizato Project, CLUSTER, Hiroshima Prefectural Institute of Industrial Science and Technology, Higashi-Hiroshima, Japan, [3]PhoenixBio Co., Ltd, Hiroshima, Japan, [4]Developmental Biology Laboratory and Hiroshima University 21st Century COE Program for Advanced Radiation Casualty Medicine, Department of Biological Science, Graduate School of Science, Hiroshima University, Higashi-Hiroshima, Japan

*Present address: PhoenixBio. Co. Ltd., 3-4-1 Kagamiyama, Higashihiroshima, Hiroshima 739-0046, Japan.
Tel: +81-82-831-0016; Fax: +81-82-831-0017

†Present address: Tokyo Women's Medical University, Institute of Advanced Biomedical Engineering and Science, Kawada-cho 8-1, Shinjuku-ku, Tokyo 162-8666, Japan. Tel: +81-3-3353-8111 (Ext. 30233); Fax: +81-3-3359-6046

Key words: bone marrow transplantation – flow cytometry – hepatocyte transplantation – humanized mice – SCID mice

Abbreviations: BMCs, bone marrow cells; m_{SCID}, SCID mouse; PBMCs, peripheral blood mononuclear cells; BMCT, bone marrow cell transplantation; *h*-Alb, human albumin; $r_{nudeF344}$, F344 nude rats; PHx, partial hepatectomy; HPCT, hepatocytes transplantation; BM, bone marrow; CYP, cytochrome P450; mAb, monoclonal antibody.

Address reprints request to Katsutoshi Yoshizato, Ph.D., PhoenixBio. Co. Ltd., 3-4-1 Kagamiyama, Higashishiroshima, Hiroshima 739-0046, Japan (E-mail: katsutoshi.yoshizato@phoenixbio.co.jp)

Received 5 May 2008;
Accepted 29 May 2008

Introduction

Hepatocytes play prime roles in metabolizing nutrients and detoxifying chemicals in the liver. Rodents, mostly rats, are used for efficacy and safety testing of new medicines. However, the patterns of drug metabolism and detoxification of rodent hepatocytes differ considerably from those of human (*h*) hepatocytes [1,2]. Therefore, *h*-hepatocytes are important for these types of studies, and as sources for hepatocyte-incorporated artificial liver devices and transplantation therapy for the treatment of patients with liver failure. However, the sources and availability of *h*-hepatocytes are rather limited.

To overcome the problems associated with *h*-hepatocytes, we created a mouse with a liver that consists of *h*-hepatocytes, using a liver-injured and immunodeficient animal as the host for *h*-hepatocyte transplantation that had been obtained by crossing an albumin (Alb) enhancer/promoter-driven urokinase-type plasminogen activator (uPA)-transgenic mouse with a severe combined immunodeficiency (SCID) mouse, the offspring being called a uPA/SCID mouse [3]. When transplanted into uPA/SCID mice, *h*-hepatocytes are engrafted and progressively repopulate the host liver, thereby generating mice with livers that consist almost completely of *h*-hepatocytes. These humanized mice mimic quite well the functions of *h*-hepatocytes, so they are useful for the testing of drug metabolism and toxicity, as well as a hepatitis B virus (HBV)- and hepatitis C virus (HCV)-susceptible animal model [3–5]. However, the small body size of this mouse limits its utilization in broader research areas, such as biology, physiology, biochemistry, pharmacy, and pharmacology. The major limitations are small total blood volume and difficulties with surgical manipulations, such as sampling of blood and bile. In addition, abundant metabolic data have been accumulated using rats in pharmacological studies.

The above-mentioned limitations led us to create "humanized" rats for studying *h*-hepatocytes *in vivo*. The advantages of humanized rats over humanized mice are as follows: (1) surgical manipulation is easier; (2) *h*-hepatocyte propagation is expected to be more than 10-fold higher; and (3) data obtained from chimeric rats can be compared with previously accumulated rat metabolic data.

In the present study, we investigated a method to generate "severe" immunodeficiency in nude rats that lack T cells. SCID mouse (m_{SCID})-bone marrow cells (BMCs) were introduced into the lethally irradiated nude rats. These rats ("SCID-rats") were subjected to retrorsine treatment and partial hepatectomy (PHx), followed by *h*-hepatocyte transplantation (*h*-HPCT). The yielded rats were characterized with respect to the engraftment, proliferation, and functions of the *h*-hepatocytes. As a result, we were able to generate the *h*-hepatocyte-bearing SCID rat whose bone marrow (BM)-related cells had been mostly (>94%) replaced with m_{SCID}-BM-derived cells, although the *h*-hepatocytes did not show a significant degree of replication.

Methods

Animals

Fischer 344 nude rats (F344/N Jcl-*rnu*/*rnu*) aged 4 weeks and SCID mice (Fox Chase SCID C.B-17/Icr-*scid*/*scid*Jcl) aged 6 weeks were purchased from CLEA Japan (Osaka, Japan). All animals were maintained under pathogen-free conditions and in compliance with the guidelines of Hiroshima University and the Hiroshima Prefectural Institute of Industrial Science and Technology.

Conditioning of F344 nude rats

Host BMCs were abrogated by whole-body X-ray irradiation of F344 nude rats [6]. The animals were exposed twice to X-rays. The first irradiation dose was fixed at 10 Gy [6]. Three days later, the rats received the second irradiation at different doses (4, 6, 8, and 10 Gy) for dosage optimization. These irradiation regimens are indicated in a simple way herein. For example, the regimen in which the second irradiation was 4 Gy is indicated as "10 + 4."

Transplantation of m_{SCID}-BMCs into conditioned rats

The m_{SCID}-BMCs were flushed out from the femurs and tibias of SCID male mice with Medium 199 (Sigma–Aldrich, Tokyo, Japan) containing 4 μg/ml gentamycin (Sigma–Aldrich) and 0.01 M Hepes buffer (Gibco, Invitrogen, Tokyo, Japan) using a 26G needle (TERUMO, Tokyo, Japan). The m_{SCID}-BMCs were mechanically resuspended in the medium by gentle aspiration through a 5-ml pipette, passed through a 40-μm-mesh nylon filter (BD Falcon, Tokyo, Japan), pelleted at 600 *g* for 5 min, and resuspended. Viable cells were counted under a microscope using the trypan blue exclusion test. The irradiated rats were transplanted with 10^8 m_{SCID}-BMCs in 500 μl of Medium 199 via the tail vein 1 day after the second irradiation. In the present study, the rats with m_{SCID}-BMCs were designated as SCID rats, since the replacement rate of the

peripheral blood mononuclear cells (PBMCs) with m_{SCID}-PBMCs was quite high (94%).

FACS analysis of hematopoietic chimerism

Blood samples (300 μl per rat) were collected using a heparinized syringe once per week after *m*-bone marrow cells transplantation (BMCT). The blood cells were lysed with ammonium chloride–potassium carbonate lysis buffer consisting of 0.15 M NH_4Cl, 10 mM $KHCO_3$, and 0.1 mM EDTA-Na_2 in 500 ml of MilliQ water, washed twice, and the final pellets containing PBMCs were suspended in FACS buffer, phosphate-buffered saline containing 1.0 mg/ml bovine serum Alb fraction V (Roche Diagnostics K.K., Tokyo, Japan) and 1.0 mg/ml sodium azide (Nacalai Tesque K.K., Kyoto, Japan). The PBMCs were resuspended in FACS buffer and divided equally into test tubes. The PBMCs were stained for 30 min at 4 °C with the following immunofluorescently labeled monoclonal antibodies (mAbs; all from BD Pharmingen, Tokyo, Japan) with specificity for the rat (*r*) or mouse (*m*): FITC-labeled *m*-anti-*r* RT1A and *r*-anti-*m*-biotinylated H-$2D^d$ for class I MHC antigens; FITC-labeled *m*-anti-*r*-CD11b/c and phycoerythrin (PE)-labeled *r*-anti-*m*-CD11b for macrophages; FITC-labeled *m*-anti-*r*-CD4 and PE-labeled *r*-anti-*m*-CD4 for CD4-T cells; PE-labeled *m*-anti-*r*-CD8 and FITC-labeled *r*-anti-*m*-CD8 for CD8-T cells; FITC-labeled *m*-anti-*r*-B220 and PE-labeled *r*-anti-*m*-CD19 for B cells; and biotinylated *m*-anti-*r*-CD161a and FITC-labeled *r*-anti-*m*-CD49/Pan for NK cells. The biotinylated mAbs were visualized with PE-labeled streptavidin for 15 min at 4 °C in the dark. Stained cells were analyzed using FAC-Scalibur (Becton Dickinson, Tokyo, Japan). Dead cells were excluded from the analysis by forward-scatter and propidium iodide (PI) staining. The FACS data were analyzed using the Win MDI software.

Isolation of *h*-hepatocytes from humanized mice

Humanized mice were generated as described previously [3]. Briefly, $7.5–10.0 \times 10^5$ cryopreserved *h*-hepatocytes from a 4-year-old boy (BD Gentest) were transplanted into uPA/SCID mice. Liver cells were isolated from the chimeric mice with >10 mg/ml *h*-Alb in their blood using the two-step collagenase perfusion method [7] and centrifuged three times at 50 *g* for 2 min. The pellet was suspended in Dulbecco modified Eagle's medium (Gibco, Invitrogen) that contained 10% fetal bovine serum, and the living cells were counted using the trypan blue exclusion test. The purity of the *h*-hepatocytes in the preparation was >90%, as determined by FACS analysis with *h*-hepatocyte-specific antibody (K8216) that had been prepared as described below. We confirmed that when transplanted into a new uPA/SCID mouse, these *h*-hepatocytes engrafted the liver, proliferated therein, and formed colonies (data not shown).

Preparation of K8216

A BALB/c mouse was immunized with 10^7 subcultured *h*-hepatocytes [8] three times weekly for 3 weeks with a booster injection of 2.5×10^7 subcultured *h*-hepatocytes after the last immunization. Frozen sections of human and murine livers were incubated with hybridoma supernatants obtained by conventional methods at the Institute of Immunology (Tokyo, Japan) and with the secondary antibodies of Alexa 488-labeled anti-*m*IgG goat sera (Molecular Probes, Invitrogen). The hybridoma for which the supernatant reacted with the plasma membranes of *h*-hepatocytes, but not with those of *m*-hepatocytes, was selected. The supernatant was analyzed by FACS for reactivity with the surfaces of hepatocytes. Thus, the *m*- and *h*-hepatocytes were incubated with the hybridoma supernatant and the secondary antibodies, and analyzed in the FACS Vantage (Becton Dickinson) using a 100-μm nozzle. Fluorescence was measured after excitation at 488 nm through a 530-nm filter (FL1) with a 4-decade logarithmic amplification. This analysis showed that the antibodies reacted with the cell surfaces of *h*-hepatocytes, but not with those of *m*-hepatocytes. The hybridoma was injected intraperitoneally (i.p.) into nude mice, and the antibodies in the ascites (designated as K8216) were purified by ammonium sulfate sedimentation.

Transplantation of *h*-hepatocytes into SCID rats

Retrorsine is used as a strong anti-mitogenic agent for rat hepatocytes [9]. *h*-Hepatocytes isolated from the chimeric mice as described above were transplanted in retrorsine- and PHx-treated rats as reported previously [9] with modifications. The m_{SCID}-BMC-bearing rats were given two i.p. injections of retrorsine (30 mg/kg body weight; Sigma–Aldrich) 2 weeks apart, to inhibit hepatocyte proliferation in the host rat liver. Histologic sections of the livers were obtained from the SCID rats 3 weeks after the second injection of retrorsine and stained with hematoxylin and eosin. These sections showed that most of the host hepatocytes had become megakaryocytes (data

not shown), reflecting the inhibition of hepatocyte cell division.

Three weeks after the second injection, the animals were anesthetized by ether inhalation and subjected to 40% PHx. The lateral right lobe was exposed by a midline incision near the xiphisternum and resected, and the incision was closed with a suture. The ileocecum was exposed by a midline incision at the hypogastric region. The *h*-hepatocytes obtained from the chimeric mice were suspended at 2.5×10^6 and 5.0×10^6 cells in 0.5-ml aliquots and transplanted into the SCID rats via the portal vein using a syringe. Murine plasma thrombin (Sigma–Aldrich) was used for hemostasis. Serum samples (50 µl) were collected from the tail vein periodically after *h*-HPCT and used for measuring *h*-Alb concentrations by ELISA (Human Albumin Sensitive ELISA Kit; Cygnus Technologies, Inc., Southport, NC, USA). In preliminary studies, to optimize the number of *h*-hepatocytes for transplantation, we obtained data showing higher rates of the engraftment and the survival of the transplanted cells in the host liver when 5.0×10^6 cells were transplanted compared with the case of transplantation of 2.5×10^6 cells. Therefore, we present herein the results of transplantation experiments with 5.0×10^6 *h*-hepatocytes.

Immunohistochemistry

The rat livers were harvested at 3 and 4 weeks after *h*-HPCT. The rats were all injected i.p. with bromodeoxyuridine (BrdU, Wako Pure Chemical Industries, Ltd., Osaka, Japan) at 10 µl/g body weight 1 h before killing. Cryosections (5-µm thickness) were fixed in cold acetone, blocked with 10% goat or donkey serum for 30 min at room temperature. Sections were incubated with *m*-anti-*h*-cytokeratin 8/18 (*h*CK8/18) mAbs (Cappel Laboratories Inc., West Chester, PA, USA), to distinguish the *h*-hepatocytes. The primary Abs were visualized with Alexa 488-labeled goat anti-*m*-IgG (Molecular Probes). As a measure of the functions of engrafted *h*-hepatocytes, cryosections were incubated with the *m*-anti-*h*-CK8/18 mAbs and rabbit anti-*h*-cytochrome P450 (CYP) 2D6 (Daiichi Pure Chemicals) or 2E1 (Affiniti) mAb (double staining). The primary Abs were visualized with Alexa 488-labeled donkey anti-*m*-IgG (Molecular Probes) or Alexa 594-labeled donkey anti rabbit-IgG. Formalin-fixed paraffin sections (5-µm thickness) were incubated with *m*-anti-*h*-cytokeratin 18 mAb (DakoCytomation) and goat anti-*h*-Alb antibody (Bethyl Laboratories) for double staining, or with goat anti-*h*-Alb antibody and *m*-anti-BrdU mAb (DakoCytomation) for double staining. The primary Abs were visualized with Alexa 488-labeled donkey anti-*m*-IgG or anti goat-IgG or Alexa 594-labeled donkey anti goat-IgG or anti-*m*-IgG (Molecular Probes). The paraffin sections were exposed to microwaves in Target Retrieval Solution (DakoCytomation), to activate the antigens. The *r*- and *m*-macrophages (Kupffer cells) were identified in the SCID rat liver as follows. Cryosections were prepared from the livers of rats at 2 and 7 weeks after m_{SCID}-BMCT, and at 3 and 4 weeks after *h*-HPCT. The sections were incubated with *r*-anti-*m*-macrophage mAb (BM8; BMA Biochemicals, Augst, Switzerland) or *m*-anti-*r*-macrophage mAb (ED2; BMA Biochemicals). The primary Abs were visualized with Alexa 488-labeled goat anti-*m*-IgG and Alexa 594-labeled goat anti-*r*-IgG (Molecular Probes). All sections were counterstained with Hoechst (bisbenzimide; Sigma–Aldrich).

RNA extraction and reverse transcription-PCR

Total RNA samples were extracted with ISOGEN (Nippon Gene, Tokyo, Japan) from the livers of normal F344 nude rats and from rats and mice both bearing *h*-hepatocyte. The RNA samples (1 µg each) were reverse-transcribed at 42 °C for 90 min in a 20-µl reaction mixture that contained random hexamers (Invitrogen) using PowerScript Reverse Transcriptase (Clontech). PCR was performed with rTaq (Takara Bio, Shiga, Japan) under the following conditions: 94 °C for 5 min, followed by 30–40 cycles of denaturing at 94 °C for 30 s, annealing at 54–60 °C for 30 s, and extension at 72 °C for 30 s. The following genes were subjected to semi-quantitative PCR under the conditions listed in Table 1 using primer sets that amplify only human gene (*h*) or mouse, rat, and human gene (*mrh*): *h*-Alb, *h*-α1-antitrypsin (*h*-AAT), *h*-glucose-6-phosphatase (*h*-G6P), *h*-hepatocyte nuclear factor 4 (*h*-HNF-4), cytochrome P450 (*h*-CYP1A2, 3A4, 2E1, 2D6) and *rmh*-glyceraldehyde-3-phosphate dehydrogenase (*mrh*-GAPDH). The amplified PCR products were analyzed by electrophoresis in 2% agarose gels (agarose 36GU; Funakoshi Co., Ltd., Tokyo, Japan) or 4% agarose gels (NuSieve 3:1 agarose; BioWhittaker Molecular Applications) and visualized under UV illumination after ethidium bromide staining.

Results

Generation of SCID rats

F344 nude rats were subjected to X-ray irradiation under the regimen described above and were transplanted 1 day later with 10^8 m_{SCID}-BMCs.

Table 1. Primer sets for RT-PCR

Gene name	Forward primers	Reverse primers	Products size (bp)	Annealing temp. (C°)	Cycles
h-Alb	tgccgaagtggaaaatgatgag	gcaagtctcagcagcagcacg	179	60	40
h-AAT	acccttttgaagtcaaggacaccg	ccattgctgaagaccttagtgatgc	360	60	40
h-G6P	tgggatccagtcaacacattac	caaaacccaccagtatggacgc	234	58	40
h-HNF-4	tcacctcccccgtctcc	Tgcgatgctggcaatctt	61	60	40
h-CYP1A2	agactgcctcctccggg	cagggttaggcaggtagcg	62	60	40
h-CYP3A4	tgtgaggaggtagatttggctc	tcaggaggagttaatggtgctaa	80	60	40
h-CYP2E1	cagcacaactctgagatatgggc	gggcatctcttgcctatcctt	132	60	40
h-CYP2D6	gtccaacaggagatcgacga	ggcatgtgagcctggtca	70	60	40
mrh -GAPDH	accacagtccatgccatcac	tccaccaccctgttgctgta	451	54	30

h, human-specific; *mrh*, mouse-, rat-, and human specific.

Table 2. Survival rates of the hosts after different X-ray dosages in the presence or absence of *m*-BMCT

Second irradiation with X-rays (Gy)	*m*-BMCT	Number of animals: Total	Dead before 7 weeks	Alive until 7 weeks	FACS analysis
0	–[a]	7	0	7	2
4	+	2	0	2	2
4	–	2	0	2	0
6	+	2	0	2	2
6	–	2	0	2	0
8	+	2	0	2	2
8	–	2	0	2	0
10	+	48	0	48	27
10	–	9	9	0	0

[a]Without *m*-BMCT.

The survival rates of the hosts under these regimens are summarized in Table 2. Irrespective of the dosage of the irradiation and the *m*-BMCT, all animals were alive beyond 7 weeks after the start of experiment including the most severe regiment except the animals that were irradiated with "10 + 10," but not received the *m*-BMCT. These rats were in severe anemia and all dead before 7 weeks. They had low body weight at the time of death, the cause of which was most likely BM failure.

We investigated the chimerism of the PBMCs in the host blood by two-color flow cytometry once a week after transplantation of the m_{SCID}-BMCs (Fig. 1). The changes in the occupancy of MHC class I^+ cells, macrophages, and NK cells after *m*-BMCT are shown in Fig. 1(A,B) for *m*- and *r*-cells, respectively. The populations of *m*-MHC class I^+ cells and macrophages increased with time post-transplantation as shown in Fig. 1(A a-1, a-2), respectively. These rates of increase became more pronounced as the second irradiation dosage was increased. The regimen "10 + 10" allowed the m_{SCID}-BMCs to repopulate almost completely the *r*-peripheral blood (94.5% *m*-MHC class I^+ cells) at 5 weeks post-*m*-BMCT (Fig. 1A a-1). Under "10 + 10," the percentages of *m*-macrophages at 1 week post-BMCT were 61.3% and increased to 93.1% at 5 weeks (Fig. 1A a-2). Originally, *m*-NK cells occupied 20–30% of the m_{SCID}-PBMC fraction. But their occupancy in the hosts was < 3% under all the tested regimens (Fig. 1A a-3), indicating that the *m*-NK cells did not proliferate therein after transplantation. As expected, the populations of *r*-MHC class I^+ cells, macrophages, and NK cells decreased with time under all the tested irradiation regimens (Fig. 1B). These rates of decrease became more pronounced as the second irradiation dosage was increased.

Similarly, we determined the changes in the occupancy of *m*- and *r*-$CD8^+$ T cells, $CD4^+$ T cells, and B cells. However, the occupancy of the *m*-cells was all quite low (<0.1%) to extract any significant conclusion. The occupancy of the *r*-cells was 2–15% and showed a tendency to decrease with the increase in the dosage of second irradiation (data not shown). From these results, we concluded that "10 + 10" is optimal for myeloablation. The level of reconstitution with m_{SCID}-BMCs reached as high as 94% under this regimen.

h-Hepatocyte-transplantation into retrorsine- and PHx-treated SCID-rats

h-Hepatocytes were isolated from chimeric mice with replacement index (RI) > 85% and, 5.0×10^6 cells each, were injected into 12 retrorsine-treated and 40% PHx SCID rats (#1–12). Rats that did not receive m_{SCID}-BMCs were similarly transplanted with *h*-hepatocytes as control animals. Eight (#1–8) were alive at least until 3 weeks (survival rate, approximately 67%). The average blood *h*-Alb levels of these rats 1 week post-*h*-HPCT were 21.8 ± 10.9 ng/ml (n = 8), which slowly increased to 29.6 ± 10.9 ng/ml (n = 8) three weeks later. Blood *h*-Alb concentrations were individually monitored for these eight animals during the experimental period as a measure of growth of *h*-hepatocyte colonies (Fig. 2). One rat (#7) died 3 weeks post-transplantation, and the remaining

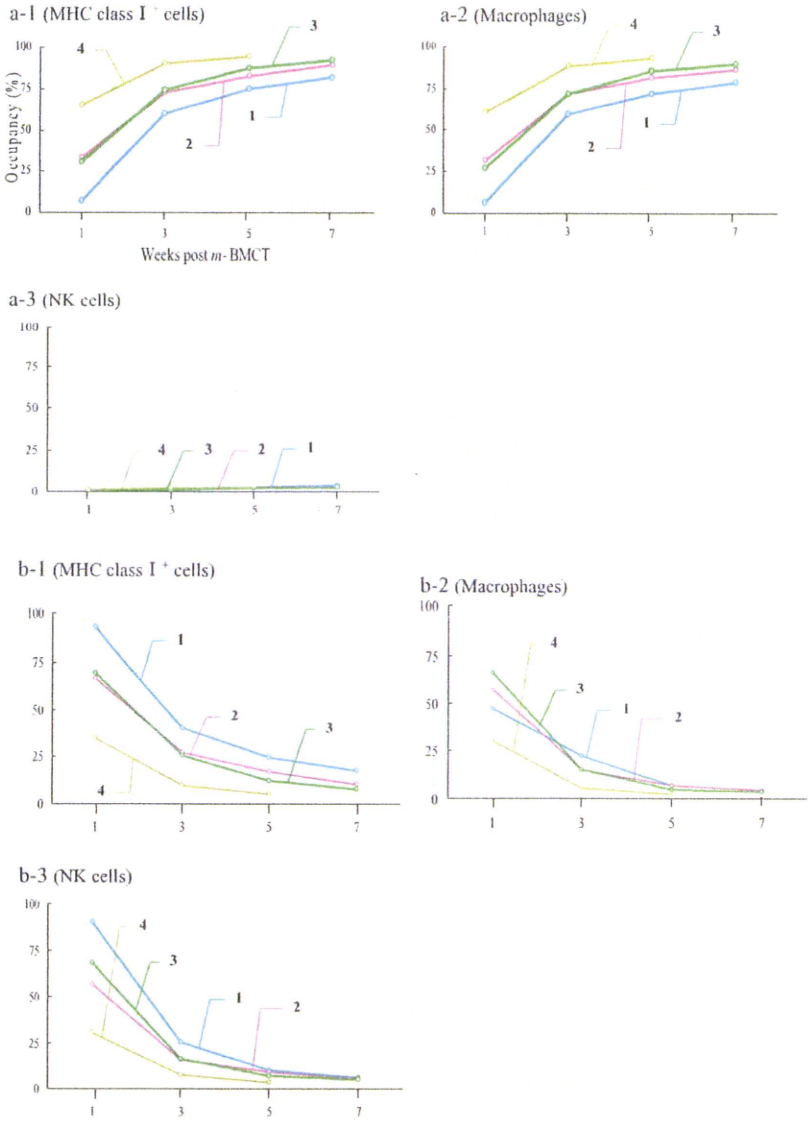

Fig. 1. Replacement of *r*-PBMCs with *m*-PBMCs by transplanting m_{SCID}-BMCs into SCID rats. F344 nude rats were subjected to four different X-ray irradiation (Gy) regimens ("10 + 4," "10 + 6," "10 + 8," "10 + 10") and transplanted with 10^8 m_{SCID}-BMCs 1 day after the second round of irradiation. The lines attached with Arabic numerals, 1, 2, 3, and 4 in the graphs represent individual rats irradiated according to "10 + 4," "10 + 6," "10 + 8," and "10 + 10" regimens, respectively. PBMCs were isolated at 1, 3, and 5 weeks post-*m*-BMCT from the rats and analyzed by two-color flow cytometry. Three types of cells were analyzed as PBMCs: MHC class I^+ cells (a-1 and b-1 for *m*- and *r*-cells, respectively), macrophages (a-2 and b-2 for *m*- and *r*-cells), and NK cells (a-3 and b-3 for *m*- and *r*-cells). *m*- and *r*-MHC class I^+ cells were detected as H-2D- and RT1A-positive ($H\text{-}2D^+$- and $RT1A^+$-) cells, respectively. *m*- and *r*-Macrophages were detected as $CD11b^+$- and $CD11b/c^+$-cells, respectively. *m*- and *r*-NK cells were detected as $CD49/Pan^+$- and *r*-$CD161a^+$-cells, respectively. The occupancy (%) of each type of cells was determined and is plotted against weeks post-*m*-BMCT. (A) Changes in the percentages of *m*-PBMCs. a-1. MHC class I^+-cells. (a-2) Macrophages. (a-3) NK cells. (B). Changes in the percentages of *r*-PBMCs. (b-1) MHC class I^+-cells. (b-2) Macrophages. (b-3) NK cells.

seven rats were kept for an additional 1 week, at which time the blood *h*-Alb levels were determined and the animals were killed. The blood *h*-Alb levels were detectable in all the tested rats at 1 week post-*h*-HPCT, thereafter these levels increased slightly but continuously to 3 weeks in four rats (#1, 2, 3, and 5). However, the levels decreased at 4 weeks post-*h*-HPCT. Animals #4 and #6 showed continuous decreases in *h*-Alb levels through 4 weeks (#4) and 3 weeks (#6) post-*h*-HPCT. Rat #1 showed an exceptionally high *h*-Alb level (95 ng/ml) at 3 weeks post-*h*-HPCT. In contrast, the blood *h*-Alb levels were undetectable during the experimental period in the unconditioned control rats that had received *h*-hepatocytes.

Expression of hepatocyte-specific genes and proteins by *h*-hepatocytes in SCID mice

RNAs were extracted for RT-PCR from the frozen liver tissues of SCID rats that had been transplanted with 5.0×10^6 *h*-hepatocytes shown in Fig. 2. Similarly, RNAs were extracted from normal nude rat livers (negative control) and from the livers of the chimeric mice transplanted with the same donor *h*-hepatocytes (positive control). All the livers of the tested SCID rats contained *h*-hepatocytes that expressed *h*-Alb, *h*-AAT, *h*-G6P, *h*-HNF-4, *h*-CYP1A2, 3A4, 2E1, and 2D6 mRNAs (Fig. 3). Liver sections prepared from the SCID rats used for RT-PCR were subjected to immunostaining for *h*-CK8/18, *h*-Alb, CYP2D6, 2E1, and BrdU

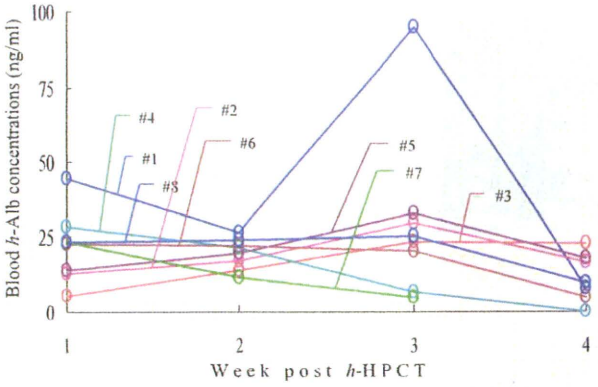

Fig. 2. Blood *h*-Alb concentrations in SCID rats post-*h*-HPCT. *h*-Hepatocytes (5.0×10^6 cells) were transplanted into the livers of retrorsine- and PHx-treated SCID rats. The *h*-Alb levels were determined in the eight rats (#1 through #8) at 1, 2, and 3 weeks. Animal #7 died 3 weeks post-*h*-HPCT. The *h*-Alb levels in the remaining seven rats were determined at 4 weeks post-*h*-HPCT.

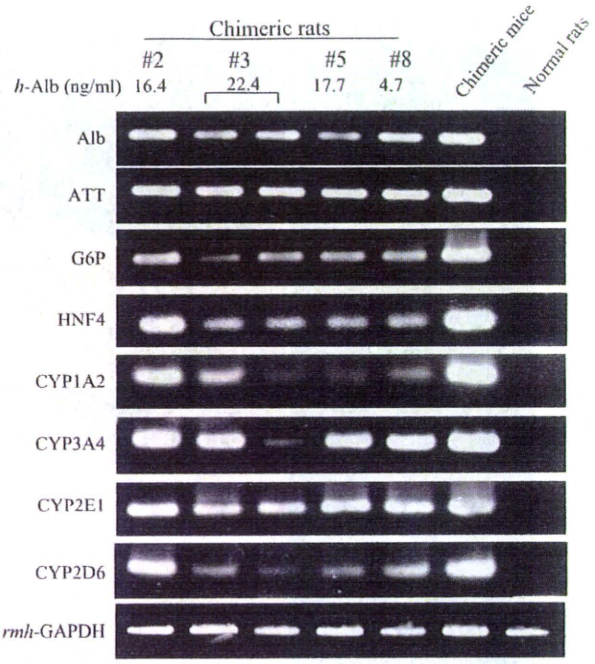

Fig. 3. Expression profiles of *h*-hepatocyte-specific genes in SCID rat livers. Total RNAs were extracted from the livers of normal nude rats and *h*-hepatocyte-chimeric SCID rats, and also from *h*-hepatocyte-chimeric mice from which the *h*-hepatocytes for transplantation into the SCID rats had been isolated. The RNA samples were subjected to PCR to measure the expression levels of the *h*-Alb, *h*-ATT, *h*-G6P, *h*-HNF-4, *h*-CYP1A2, 3A4, 2E1, and 2D6 genes. GAPDH mRNAs were measured as the reference, to ensure equivalent amounts of the tested RNA were used with primers common to the rat, human, and mouse species. Animals #2, 3, 5, and 8 indicated below the "Chimeric rats" tag correspond to the animals #2, 3, 5, and 8 shown in Fig. 2. The blood *h*-Alb concentrations of the tested animals are shown at the tops of the panels.

(Fig. 4). The *h*-CK18$^+$ cells expressed *h*-Alb (Fig. 4a–c). The *h*-CK8/18$^+$ colonies expressed CYP2D6 (Fig. 4d–f) and 2E1 (Fig. 4g–i). BrdU$^+$ cells were observed in *h*-Alb$^+$ cells (Fig. 4j–l). These results suggest that some of the engrafted *h*-hepatocytes are in the S-phase of the cell cycle, and that the engrafted *h*-hepatocytes are able to maintain normal functions in the rat liver tissues. The engrafted *h*-hepatocyte were able to frequently form colonies containing greater than five hepatocytes in all the tested seven animals at 4 weeks post-*h*-HPCT. There were some colonies that contained more than 10 cells in five animals.

Macrophage activation in *h*-hepatocyte-transplanted SCID rat livers

Recently, liver reticuloendothelial macrophages (Kupffer cell) were reported to reject xenogeneic cells through the interspecies incompatible CD47 signaling [10,11]. At 5 weeks post-*m*-BMCT most (~94%) of the macrophages in the PBMCs were derived from the SCID mice (Fig. 1). X-ray irradiated nude rats were transplanted with m_{SCID}-BMCs and liver tissues were removed at early (2 weeks) and late (7 weeks) time-points post-*m*-BMCT. Double-immunostaining was performed to detect and localize *m*- and *r*-macrophages in the liver sections, using the BM8 and ED2 antibodies, respectively (Fig. 5a,b). Both ED2$^+$-*r*-green and BM8$^+$-*m*-red macrophages (Kupffer cells) were scattered throughout the liver at 2 weeks post-*m*-BMCT (Fig. 5a). The ED2$^+$ cells were considered to be dying *r*-macrophages likely due to the X-ray-induced damages because they showed abnormal morphology and weak fluorescence. Although both *r*- and *m*-macrophages were similarly observed throughout the liver at 7 weeks post-*m*-BMCT, ED2$^+$-cells appeared that were morphologically normal and had brighter fluorescence than those at 2 weeks (Fig. 5b). These cells were considered to be *r*-macrophages that escaped X-ray-induced damage and had repopulated the host liver or some X-ray-resistant host progenitor cells had differentiated into macrophages.

Similar double-immunostaining was carried out for the seven *h*-hepatocyte-bearing rats #1–8 as shown in Fig. 2 that had been transplanted with *h*-hepatocyte at 11 weeks post-*m*-BMCT. The liver tissues from these animals at 4 weeks post-*h*-HPCT were used for immunostaining. These seven rats were classified into two groups according to the blood level of *h*Alb. One was the group of three rats (#2, 3, 5) that showed *h*Alb > 15 ng/ml at 4 weeks post-HPCT and the other was that of four rats (#1, 4, 6, 8) with *h*Alb < 10 ng/ml. We